Geochemistry Geophysics Geosystems G3
AN ELECTRONIC JOURNAL OF THE EARTH SCIENCES
Published by AGU and the Geochemical Society

Article
Volume 4, Number 8
12 August 2003
8913, doi:10.1029/2002GC000421
ISSN: 1525-2027

Sr-Nd-Pb composition of Mesozoic Pacific oceanic crust (Site 1149 and 801, ODP Leg 185): Implications for alteration of ocean crust and the input into the Izu-Bonin-Mariana subduction system

Folkmar Hauff, Kaj Hoernle, and Angelika Schmidt
GEOMAR, Wischhofstrasse 1-3, 24148 Kiel, Germany (fhauff@geomar.de; khoernle@geomar.de)

[1] We report Sr, Nd and Pb isotopic compositions of sediments and variably altered igneous rocks from ODP Site 801 (Marianas) and ODP Site 1149 (Izu-Bonin). These Sites provide the most complete drilled ocean crust sections located in front of the Mariana and Izu-Bonin trenches and characterize the unmodified isotopic input into these subduction zones. The subducted ocean crust belongs to the oldest (130–167 Ma) in situ Pacific Ocean crust and thus has end-member character with respect to alteration and sediment load. The lithostratigraphic division of sedimentary units at Site 1149 into clays, cherts, lower clays and carbonates with clay is reflected on isotope correlation diagrams. The Pb isotope data of the sediments show much greater variation than previously reported from this region. Particularly noteworthy are zeolite-bearing clays and clay bearing carbonates from the lower Units that have Pb isotopic compositions identical to the Izu Volcanic Front. The basaltic basement samples display variable $^{87}Sr/^{86}Sr$ ratios at near constant $^{143}Nd/^{144}Nd$ ratios, indicating mixing with seawater derived Sr. Most basaltic samples from Site 1149 and 801 exhibit highly variable $^{206}Pb/^{204}Pb$ (17.88–20.00) at near constant $^{207}Pb/^{204}Pb$ and $^{208}Pb/^{204}Pb$ ratios. Three samples from Site 801 display the most extreme $^{206}Pb/^{204}Pb$ (23.70–26.86) and $^{207}Pb/^{204}Pb$ (15.73–15.83) ratios ever measured in altered MORB reflecting an increase of $^{238}U/^{204}Pb$ ratios (μ), most likely through addition of seawater derived U. Initial Pb isotopes of most samples overlap with the age corrected field of the Pacific MORB source, thus the increase in μ took place shortly after formation of the crust in most samples. According to our new isotope data the radiogenic end-member of the Izu arc volcanic rocks could either represent Pb from the lower sediment column released from the slab by delayed dewatering or an integrated slab fluid in which 90–95% of the Pb comes from the basaltic crust and 5–10% of the Pb from the sediments. The Pb isotope systematics of the Mariana arc output suggest two component mixing. Both components appear to be input derived with the radiogenic component represented by average Site 801 sediment and the unradiogenic component generated by mixing of ~80% unaltered crust with ~20% highly altered crust.

Components: 17,517 words, 8 figures, 5 tables.

Keywords: Subduction factory; Ocean Drilling Program; Leg 185; Izu-Mariana; Sr-Nd-Pb-isotopes; seafloor alteration.

Index Terms: 1040 Geochemistry: Isotopic composition/chemistry; 1030 Geochemistry: Geochemical cycles (0330); 1020 Geochemistry: Composition of the crust.

Received 14 August 2002; **Revised** 16 March 2003; **Accepted** 4 June 2003; **Published** 12 August 2003.

Hauff, F., K. Hoernle, and A. Schmidt, Sr-Nd-Pb composition of Mesozoic Pacific oceanic crust (Site 1149 and 801, ODP Leg 185): Implications for alteration of ocean crust and the input into the Izu-Bonin-Mariana subduction system, *Geochem. Geophys. Geosyst.*, *4*(8), 8913, doi:10.1029/2002GC000421, 2003.

Theme: Oceanic Inputs to the Subduction Factory **Guest Editors:** Terry Plank and John Ludden

1. Introduction

[2] Subduction of oceanic lithosphere at convergent plate margins causes arc volcanism and recycles surface material into the deep mantle. Because the physical and chemical changes within the subducting plate and mantle wedge are largely inaccessible, geochemical investigations concentrate on the input and output signals. While the output of island arcs has been studied extensively over the past decades [*Hawkesworth and Ellam*, 1989; *Hawkesworth et al.*, 1991; *Pearce et al.*, 1995; *Turner et al.*, 1997; *You et al.*, 1996; *Chan et al.*, 1999]., the input signal is less well known because few drill holes near trenches have reached significant penetration depths and recovery of the igneous portion of the ocean crust has been poor. The Izu-Bonin-Mariana arc system has become one of the focus regions of subduction zone research, because (1) it is an intra oceanic arc system, which minimizes the effects of crustal contamination, (2) the output of these arcs is well known [e.g., *Crawford et al.*, 1981; *Hole et al.*, 1984; *Woodhead and Fraser*, 1985; *Stern et al.*, 1988; *Elliott et al.*, 1997; *Gill et al.*, 1992; *Taylor et al.*, 1992; *Lee et al.*, 1995; *Ishikawa and Tera*, 1999; *Hochstaedter et al.*, 2000, 2001; Schmidt et al., manuscript in preparation, 2003] and (3) the angle of subduction changes along strike of the arc from 45° in Japan to 60–70° in the Central Izu arc to 90° in the Marianas [*Carlson and Mortera-Gutierrez*, 1990; *Chiu et al.*, 1991; *Van der Hilst and Seno*, 1993] allowing us to assess the influence of the structure of subduction systems on the geochemistry of the output.

[3] Drilling and seismic records reveal that the subduction input into the Izu-Mariana arc system is highly variable [*Abrams et al.*, 1993; *Abrams*, 2002]. In general, the sediment sections consist of various mixtures of red clays, brown clays, cherts, radiolarites, chalks, marls, limestones, volcaniclastic sediments and turbidites in various diagenetic stages and thickness. The major differences between the Izu and Mariana arcs with respect to sedimentary input are the exclusive occurrence of a 200 m thick volcaniclastic layer in front of the Mariana arc and the restriction of carbonate-rich lithologies in front of the Izu arc. These differences are due to differences in the plate evolution such as the proximity of Site 801 to the Magellan Seamounts, a domain of Cretaceous ocean island basalts, and the initial sedimentation depths of Site 1149 above the CCD. The investigations of *Abrams et al.* [1993] and *Abrams* [2002] reveal that the drilled strata are representative of the regional stratigraphy. Concerning Site 1149 (Abrams, personal communication) the thickness of the cherts decreases while the thickness of the clays increases in northward. The total thickness of the subducted sediment, however, stays more or less constant. Strong links between the lithology and geochemistry exist for most sediments [*Plank and Langmuir*, 1998]. Because the subducted ocean crust beneath the Izu-Mariana arc is the oldest in situ Pacific ocean crust, its igneous portion has end-member character with respect to alteration and density. Various alteration processes modify the chemical composition of the ocean crust after its formation. Hydrothermal alteration of the lowermost basaltic and gabbroic crust primarily occurs near the spreading center, but can also occur later in the history of the crust in connection with younger igneous events. Low temperature alteration can occur throughout the history of the ocean crust. This study reports Sr, Nd and Pb isotopic compositions of sediments and variably altered igneous rocks from ODP Site 801 (Marianas) and ODP Site 1149 (Izu-Bonin). These Sites provide the most complete ocean crust sections in these areas and are located in front of the Mariana and Izu-Bonin trenches, providing an excellent opportunity to characterize the unmodified isotopic input into these subduction zones (Figure 1).

1.1. Geological Background and Lithostratigraphy of ODP Sites 801 and 1149

[4] The westernmost Pacific plate East of Japan and the Marianas represents the primary input

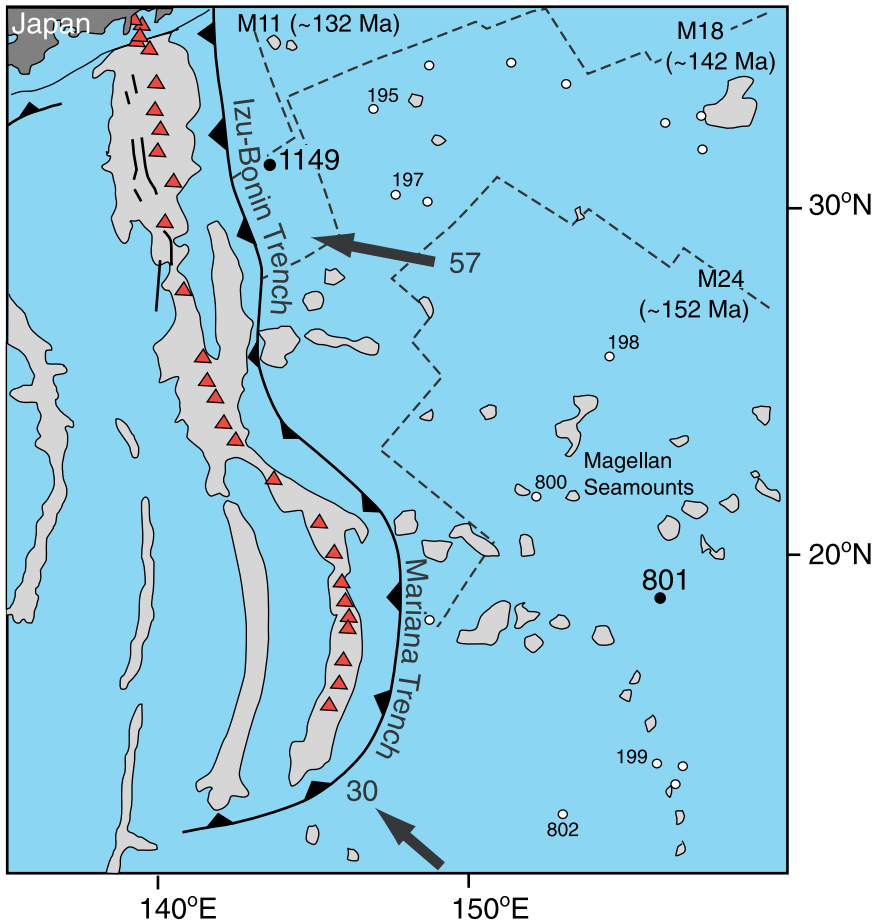

Figure 1. Westernmost Pacific off the Izu-Bonin-Mariana subduction zone. Red triangles mark the presently active volcanic front. Stippled lines trace magnetic lineations on the ocean floor. The samples from this study come from ODP Sites 1149 and 801 (filled circles). Open circles denote other DSDP/ODP drill Sites. Magnetic lineations after *Nakanishi et al.* [1989, 1992], *Channell et al.* [1995], *PLATES Project* [1998]; Plate motions after *DeMets et al.* [1990], *Seno et al.* [1993] and *Stern and Klemperer* [2003].

into the Izu-Bonin-Mariana subduction system (Figure 1). Magnetic lineations [*Nakanishi et al.*, 1989, 1992; *Channell et al.*, 1995; *PLATES Project*, 1998], radiometric age dating [*Pringle*, 1992] and biostratigraphy [*Matsuoka*, 1992; *Ogg et al.*, 1992; *Bartolini and Larson*, 2001] show an age progression from Middle Cretaceous (~127 Ma, magnetic lineation M5) in the North (east of southern Japan) to Middle Jurassic (~165–170 Ma, Jurassic Magnetic Quiet Zone) in the South (east of the southern Marianas), representing the oldest in situ oceanic crust of the Pacific basin. Numerous Deep Sea Drilling Project/Ocean Drilling Program (DSDP/ODP) cruises (Legs 6, 7, 17, 20, 32, 33, 60, 61, 89, 129, 185) have sampled this part of the Pacific over the past 30 years (Figure 1). The most complete sediment and igneous ocean crust sections on the subducting Pacific plate of the Izu-Bonin-Mariana subduction system were sampled during ODP Leg 129 [*Lancelot et al.*, 1990] and ODP Leg 185 [*Plank et al.*, 2000].

[5] Leg 129 drilled through on average 500 m of Quaternary through Jurassic sediments at Sites 800, 801 and Quaternary through Cretaceous sediments at Site 802 (461.6–493.7 m at Site 801) as well as 100 m of Jurassic igneous basement at Site 801 [*Lancelot et al.*, 1990]. Hole 801C was reentered during ODP Leg 185 and deepened to 936 meters below seafloor (mbsf), making it so far the deepest hole ever drilled into old [~167 Ma *Pringle*, 1992] Pacific ocean crust [*Plank et al.*,

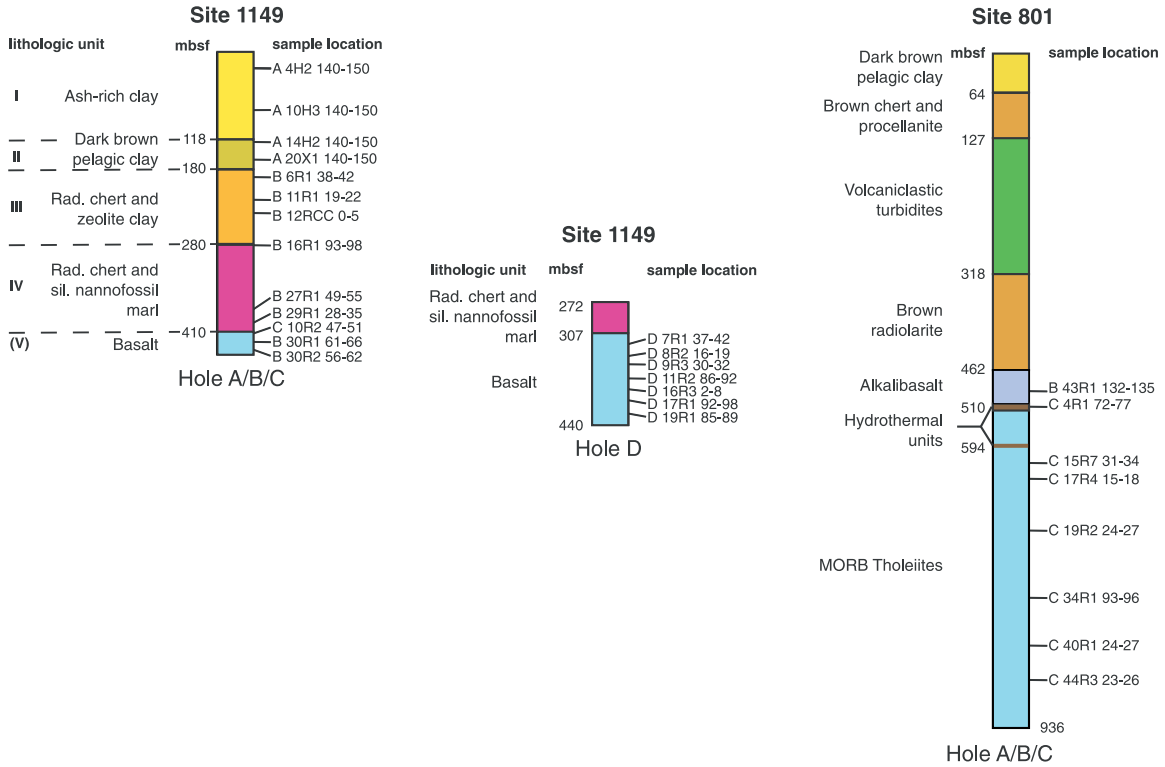

Figure 2. Simplified lithostratigraphic sections of ODP Site 1149 and 801. Modified from *Plank et al.* [2000].

2000]. The lithostratigraphy at Site 801 (Figure 2) from top to bottom comprises 64 m of pelagic clay, 63 m chert-porcelanite, 192 m volcaniclastic turbidites from the Magellan Seamounts, 125 m cherts, 20 m of Callovian radiolarites and claystones and 65 m of ~157 Ma [*Pringle*, 1992] alkali-basaltic sills intercalated with chert-rich sediments. The igneous basement begins at 510 mbsf with a ~20 m Si and Fe oxyhydroxide-rich hydrothermal unit, followed by variably altered ~167 Ma tholeiitic basalts (sheet and pillow lavas), hyaloclastites and breccias to the base of Site 801. A second Si and Fe oxyhydroxide-rich hydrothermal unit occurs at 595–626 mbsf. Within the tholeiitic section thick intervals alternate unsystematically with thin flow units, brecciated intervals and hyaloclastites.

[6] As summarized in Figure 2, Site 1149 recovered from top to bottom 118 m Late Pliocene to Late Miocene carbonate-free clays (unit I), 62 m dark brown pelagic clays (unit II) of unknown age, 100 m interbedded radiolarian chert, porcelanite and siliceous clay (unit III) of unknown age and 130 m Late Cretaceous interbedded radiolarian chert and radiolarian nannofossil chalk and marl (unit IV). The igneous basement consists of 133 m of ~130 Ma tholeiitic basalt. In contrast to Site 801, thin flow units dominate the basement at Site 1149.

[7] Alteration and veining of the igneous basement differs in Sites 801 and 1149. Alteration in Hole 801C mostly reflects low temperature (0–50°C) basalt-seawater interaction and is thus very similar to upper oceanic crust alteration observed elsewhere. Most basalts are gray, slightly but pervasively altered and contain secondary minerals which are mainly saponite ($(Mg_3(OH)_2Ca_{0.5}nH_2O)$, calcite and celadonite ($K(Mg, Fe^2)(Fe^3, Al)(OH)_2[Si_4O_{10}]$) replacing olivine and filling pore spaces. Nevertheless, fresh glass rims are preserved throughout the hole. In conjunction with four locally distinct zones of increased alteration right next to less altered sections, it is evident that the degree of alteration does not necessarily correlate with depth but may alternate between zones with oxidizing conditions (high fluid/rock ratios) and zones with anoxic conditions. The most intense alteration in Hole 801C occurs adjacent to the

hydrothermal units. Here the igneous material is pale green and bleached and all ferromagnesian minerals are destroyed. The replacement of primary minerals by calcite, smectite and celadonite causes an increase of alkalis and a loss of Mg, Fe and trace metals. A similar grade and degree of alteration is present in most breccias and hyaloclastites. Thick (up to 2.5 cm) veins occur in several orientations and generations and are made up of combinations of calcite, saponite, celadonite, iron oxides or sulfides, and silica (quartz and chalcedony) whereby carbonate and saponite dominate. The veins are commonly surrounded by variably colored, but mainly dark, alteration halos. Here celadonite-nontronite assemblages fill pore space and replace olivine whereas abundant disseminated iron oxyhydroxides replace interstitial material. Just outside the halo interstitial material is replaced by disseminated pyrite.

[8] In contrast to Site 801, low-temperature alteration of the igneous basement is much more extensive at Site 1149. Here the host rocks generally exhibit variably intense dusky red to dark red colors and display gray to brown mottling. Veins are generally more common but the dominant vein minerals calcite, saponite and celadonite are identical. Carbonate-rich veins are generally thicker (1.5 mm) and have wider associated halos (~6 mm), whereas saponite-rich veins are thinner (~0.3 mm) and associated with narrower halos (4 mm). In addition some reddish veins containing a mixture of Fe oxyhydroxides and clays occur.

1.2. Sample Selection and Analytical Methods

[9] A total of 117 samples from Site 801 and 35 samples from Site 1149 were selected by the ODP Leg 185 shipboard scientific party for interlaboratory geochemical analyses (see *Plank et al.* [2000] for sampling strategy). From these a high priority subset reflecting the major rock types, alteration styles and mineral end-members was assigned for isotope analyses with emphasis on 14 basement samples from Site 801, 10 basement samples and 15 sediment samples from Site 1149. From the subset we have chosen 10 basement and 10 sediment samples from Site 1149 and 8 basement samples from Site 801 for Sr-Nd-Pb isotope analyses (Table 1).

[10] Because the unmodified subduction input is of interest, unleached powders were dissolved in a hot HF-HNO_3 mixture followed by ion exchange procedures described in *Hoernle and Tilton* [1991]. Isotopic ratios were determined on a Finnigan MAT262 RPQ^{2+} Thermal Ionization Mass Spectrometer (TIMS) at GEOMAR, operating in static mode for Sr and Pb and in multidynamic mode for Nd, Sr and Nd isotopic ratios are normalized within run to $^{86}Sr/^{88}Sr = 0.1194$ and $^{146}Nd/^{144}Nd = 0.7219$ respectively and all errors are 2 sigma. Over the course of this study NBS 987 gave $^{87}Sr/^{86}Sr = 0.710210 \pm 0.000015$ (n = 9), $^{143}Nd/^{144}Nd = 0.511844 \pm 0.000011$ (n = 19) for La Jolla and $^{143}Nd/^{144}Nd = 0.511705 \pm 0.000011$ (n = 9) for our in-house SPEX Nd monitor. $^{87}Sr/^{86}Sr$ ratios are normalized to $^{87}Sr/^{86}Sr = 0.71025$. NBS 981 (n = 31) gave $^{206}Pb/^{204}Pb = 16.899 \pm 0.008$, $^{207}Pb/^{204}Pb = 15.438 \pm 0.011$, $^{208}Pb/^{204}Pb = 36.532 \pm 0.035$ and corrected to the NBS 981 values given in *Todt et al.* [1996]. Total chemistry blanks were <100 pg for Sr, Nd and Pb and thus considered negligible. Pb replicate analyses were performed on 10 samples and are generally better than 0.03% per a.m.u. (atomic mass unit) except for sample 1149D 7R1 37–42, that was reproduced within 0.05% per a.m.u.

2. Analytical Results

[11] Sr-Nd-Pb isotopic ratios of this study are shown in Tables 1–3. The data presentation follows a subdivision into layer 1 (sediments) from Site 1149 and layer 2a (fresh and altered basalt, veins, breccias) from Site 1149 and Hole 801C.

2.1. Sediments: Site 1149

[12] A total of 10 sediment samples from the A and B Holes at Site 1149 were analyzed. According to the visual core description (VCD) and smear slide analysis given in the initial report [*Plank et al.*, 2000], the samples are classified into 3 main lithological groups: clays, cherts and carbonates. Note that the samples are often mineralogically impure due to their natural origin.

Table 1. Sample Descriptions of Investigated Samples[a]

Sample (Unit)	Sample Description	Color	Texture/Structure	Classification
		Sediments		
1149A 4H2 140–150 (I)	pelagic clay	greenish grey	homogeneous	upper clay
1149A 10H3 140–150 (I)	ash-bearing siliceous clay	very dark grayish brown, black fleck and splotches	fleck and splotch	ash-bearing upper clay
1149A 14H2 140–150 (IIa)	pelagic clay	pale brown	homogeneous	upper clay
1149A 20X1 140–150 (IIb)	silt-bearing pelagic clay	brown with yellow and dark brown mottles	mottled	upper clay
1149B 6R1 38–42 (III)	radiolarian chert	dark with strong brown deformed bands	deformed	chert
1149B 11R1 19–22 (III)	radiolarian chert and radiolarian porcellanite	light brown	partly laminated	chert
1149B 12R CC 0–5 (III)	zeolite-bearing clay	chocolate brown	drilling breccia	lower clay
1149B 16R1 93–98 (IV)	clay, ash and radiolarian bearing nannofossil marl	light brown to pinkish	structureless	carbonate with clay
1149B 27R1 49–55 (IV)	clay-bearing nannofossil chalk	light reddish brown	laminated	carbonate with clay
1149B 29R1 28–35 (IV)	nannofossil marl	brown with dusky red banding	banded	carbonate with clay
		Basement		
1149B 30R1 61–66	breccia of basalt clasts in carbonate matrix	basalt: grey, matrix: white	breccia	breccia
1149B 30R2 56–62	basalt with well-developed halo and calcite and smectite vein	basalt: reddish grey, halo: bluish grey	massive	basalt
1149C 10R2 47–51	minimally altered basalt	dark grey	basalt	basalt
1149D 7R1 37–42	smectite altered hyaloclastite	dark green, some white calcite filings	brittle	hyaloclastite
1149D 8R2 16–19	interflow material of calcite and quartz	white and green	granular	inter flow material
1149D 9R3 30–32	basalt with various colored halos	basalt: reddish; halos: green, orange and brown	basalt	basalt
1149D 11R2 86–92	basalt clasts in calcite matrix	basalt: dark grey; matrix: white	breccia	breccia
1149D 16R3 2–8	minimally altered basalt	grey	homogeneous	basalt
1149D 17R1 92–98	breccia with calcite veins	dark grey with white	breccia	breccia
1149D 19R1 85–88	minimally altered basalt	dark grey	homogeneous	basalt
801B 43R1 132–135	minimally altered alkalibasalt	flecked medium grey	massive	alkalibasalt
801C 4R1 72–77	hydrothermal deposit	yellow-ochre with minor colorless silica in pore space	relict sedimentary lamination	hydrothermal unit
801C 15R7 31–34	greenish altered basalt	pale green, bleached	massive pillow interior	basalt
801C 17R4 15–18	basalt clasts in calcite and smectite	basalt: dark grey; matrix: mainly dark green, minor white	inter flow material	inter flow material
801C 19R2 24–27	hyaloclastite with palagonite and calcite matrix	basalt: dark grey; matrix: dark grey and white	hyaloclastite	hyaloclastite
801C 34R1 93–96	fresh basalt	grey	massive	basalt
801C 40R1 24–27	breccia of basalt clasts in calcite matrix	basalt: grey; matrix: white with minor green parts	breccia	breccia
801C 44R3 23–26	basalt with dark halo and calcite vein	basalt: greenish; halo: dark green	massive	basalt

[a] The samples are a subset from the high priority common samples selected by the the ODP Leg 185 shipboard scientific party.

Table 2a. Measured and Initial Sr Isotope Data of ODP Site 1149 and 801 Samples[a]

Sample	Age, Ma	Rb	Sr	$^{87}Rb/^{86}Sr$	$^{87}Rb/^{86}Sr$	±2σ	$^{87}Rb/^{86}Sr_{in}$	Propagated 2σ
				1149A				
1149A 4H2 140–150	5	98.8	130	2.20	0.711255	(8)	0.71110	
1149A 10H3 140–150	10	71.9	143	1.45	0.707982	(6)	0.70778	
1149A 14H2 140–150	19	97.1	112	2.49	0.711782	(10)	0.71111	
1149A 20X1 140–150	44	120.5	203	1.72	0.712182	(8)	0.71111	(22)
				1149B				
1149B 6R1 38–42	47	16.2	32	1.48	0.712081	(6)	0.71110	(20)
1149B 11R1 19–22	70	19.1	34	1.63	0.714509	(7)	0.71289	(69)
1149B 12RCC 0–5	90	76.8	161	1.38	0.712861	(6)	0.71110	(36)
1149B 16R1 93–98	100	44.6	229	0.56	0.709358	(8)	0.708556	
1149B 27R1 49–55	120	12.3	483	0.07	0.707567	(6)	0.707442	
1149B 29R1 28–35	120	22.1	288	0.22	0.708074	(7)	0.707695	
1149B 30R1 61–66	130	25.7	117	0.63	0.706380	(8)	0.705212	(24)
1149B 30R2 56–62	130	19.1	115	0.48	0.703958	(7)	0.703065	
				1149C				
1149C 10R2 47–51	130	2.5	122	0.06	0.702880	(8)	0.702770	
				1149D				
1149D 7R1 37–42	130	51.9	50	2.99	0.711516	(6)	0.705985	(111)
1149D 8R2 16–19	130	2.7	146	0.05	0.707437	(8)	0.707337	
1149D 9R3 30–32	130	15.9	119	0.39	0.703486	(8)	0.702774	
1149D 11R2 86–92	130	7.9	124	0.19	0.705314	(8)	0.704972	
1149D 16R3 2–8	130	4.2	179	0.07	0.702876	(8)	0.702750	
1149D 17R1 92–98	130	17.3	150	0.33	0.704165	(8)	0.703547	
1149D 19R1 85–89	130	5.9	133	0.13	0.704179	(9)	0.703940	
				801B				
801B 43R1 132–135	157	36.6	350	0.30	0.704259	(6)	0.703585	
				801C				
801C 4R1 72–77	167	0.2	2	0.39	0.707849	(11)	0.706927	(19)
801C 15R7 31–34	167	4.3	159	0.08	0.703437	(8)	0.703251	
801C 17R4 15–18	167	113.2	31	10.50	0.725724	(8)	0.700798	(499)
801C 19R2 24–27	167	30.7	44	2.00	0.709893	(7)	0.705147	(95)
801C 34R1 93–96	167	4.7	118	0.11	0.703111	(8)	0.702840	
801C 40R1 24–27	167	18.7	117	0.46	0.705006	(7)	0.703913	(22)
801C 44R3 23–26	167	8.8	133	0.19	0.703578	(8)	0.703123	

[a] Internal errors of the measured data refer to the last significant digit(s). Initial isotope ratios are calculated using element concentration data from *Kelley et al.* [2003]. For some samples the analytical uncertainties of the trace element analyses propagate to errors for the initial $^{87}Sr/^{86}Sr$ calculation that exceed the external reproducibility of Sr isotope analyses. For these samples the propagated errors are listed seperately.

[13] Three out of four pelagic clay samples from unit I and II (uppermost 180 m at Site 1149) are identical within errors in Nd-Pb isotopic composition ($^{143}Nd/^{144}Nd$ = 0.51231–0.51233, $^{206}Pb/^{204}Pb$ = 18.61–18.62). The $^{87}Sr/^{86}Sr$ isotope ratio in these samples is more variable and ranges between $^{87}Sr/^{86}Sr$ = 0.7113–0.7122. The $^{87}Sr/^{86}Sr$ ratios correlate positively with $^{87}Rb/^{86}Sr$ and therefore the differences may reflect radiogenic ingrowth of ^{87}Sr. Ash-bearing clay sample 1149A 10H3 140–150 is somewhat exceptional because it has lower $^{87}Sr/^{86}Sr$ (0.7080) and $^{206}Pb/^{204}Pb$ (18.59) but higher $^{143}Nd/^{144}Nd$ (0.51247), consistent with mixing of volcanic ash with the clay (Figures 3 and 4 and Tables 2a–2c).

[14] Two radiolarian chert samples from unit III were investigated. They have similar $^{143}Nd/^{144}Nd$ = 0.51225–0.51231, $^{206}Pb/^{204}Pb$ (19.01–19.05), $^{207}Pb/^{204}Pb$ (15.63–15.64), and $^{208}Pb/^{204}Pb$ (38.64–38.73) but variable $^{87}Sr/^{86}Sr$ (0.7121–0.7145). The cherts have more radiogenic $^{87}Sr/^{86}Sr$ and $^{206}Pb/^{204}Pb$ ratios at similar $^{143}Nd/^{144}Nd$, $^{207}Pb/^{204}Pb$ and $^{208}Pb/^{204}Pb$ ratios to the pelagic

Table 2b. Measured and Initial Nd Isotope Data of ODP Site 1149 and 801 Samples[a]

Sample	Age, Ma	Sm	Nd	$^{147}Sm/^{144}Nd$	$^{143}Nd/^{144}Nd$	±2σ	$^{143}Nd/^{144}Nd_{in}$	εNdt
				1149A				
1149A 4H2 140–150	5	4.6	21.6	0.128	0.512334	(9)	0.512330	−5.89
1149A 10H3 140–150	10	4.2	18.1	0.139	0.512465	(6)	0.512456	−3.30
1149A 14H2 140–150	19	4.63	21.92	0.127	0.512311	(7)	0.512295	−6.21
1149A 20X1 140–150	44	53.1	226.3	0.141	0.512321	(8)	0.512280	−5.87
				1149B				
1149B 6R1 38–42	47	2.6	12.5	0.124	0.512307	(7)	0.512269	−6.03
1149B 11R1 19–22	70	2.7	12.6	0.129	0.512252	(8)	0.512193	−6.93
1149B 12RCC 0–5	90	13.1	64.1	0.123	0.512289	(6)	0.512217	−5.96
1149B 16R1 93–98	100	7.4	37.9	0.118	0.512511	(8)	0.512434	−1.48
1149B 27R1 49–55	120	1.8	10.0	0.111	0.512262	(9)	0.512175	−6.02
1149B 29R1 28–35	120	3.7	20.1	0.112	0.512305	(2)	0.512217	−5.21
1149B 30R1 61–66	130	2.3	6.6	0.212	0.513178	(7)	0.512998	10.28
1149B 30R2 56–62	130	3.5	9.8	0.214	0.513185	(9)	0.513003	10.39
				1149C				
1149C 10R2 47–51	130	3.9	10.9	0.212	0.513192	(7)	0.513012	10.55
				1149D				
1149D 7R1 37–42	130	1.5	4.4	0.203	0.513146	(9)	0.512973	9.80
1149D 8R2 16–19	130	0.5	1.4	0.203	0.513156	(12)	0.512983	10.00
1149D 9R3 30–32	130	3.8	11.4	0.203	0.513167	(9)	0.512994	10.22
1149D 11R2 86–92	130	3.5	10.6	0.198	0.513128	(12)	0.512960	9.54
1149D 16R3 2–8	130	4.1	13.4	0.183	0.513100	(14)	0.512944	9.24
1149D 17R1 92–98	130	5.1	16.6					
1149D 19R1 85–89	130	5.3	15.9	0.200	0.513147	(8)	0.512977	9.87
				801B				
801B 43R1 132–135	157	5.3	24.9	0.129	0.512941	(6)	0.512809	7.27
				801C				
801C 4R1 72–77	167	0.1	0.5	0.122	0.512369	(15)	0.512236	−3.65
801C 15R7 31–34	167	4.3	12.6	0.205	0.513126	(9)	0.512902	9.34
801C 17R4 15–18	167	0.9	2.5	0.209	0.513199	(14)	0.512971	10.69
801C 19R2 24–27	167	0.3	0.5	0.304	0.513340	(21)	0.513008	11.42
801C 34R1 93–96	167	5.6	16.4	0.206	0.513154	(5)	0.512929	9.87
801C 40R1 24–27	167	3.4	9.8	0.209	0.513127	(9)	0.512899	9.28
801C 44R3 23–26	167	4.7	13.5	0.208	0.513131	(6)	0.512903	9.37

[a] Internal errors of the measured data refer to the last significant digit(s). Initial isotope ratios calculated using element concentration data from *Kelley et al.* [2003]. Propagated error taking the analytical uncertainties of the trace element data into account are within analytical error of the $^{143}Nd/^{144}Nd$ determination.

clays of unit I and II (Figures 3 and 4). Clay (e.g., sample 1149B 12RCC 0–5) is also present in Unit III. It is noteworthy that this zeolite-bearing clay is not only mineralogically distinct from the clay of unit I and II but also has considerably less radiogenic Pb isotopic ratios ($^{206}Pb/^{204}Pb$ = 18.52; $^{207}Pb/^{204}Pb$ = 15.55; $^{208}Pb/^{204}Pb$ = 38.35, Figure 4) but similar Sr and Nd isotopic compositions to the non ash-bearing upper clay samples (Figure 3). We note that the Pb isotopic composition of this sample overlaps with the Pb isotope ratios from the volcanic front of the Izu Arc [*Taylor and Nesbitt*, 1998; *Hochstaedter et al.*, 2001; Schmidt et al., manuscript in preparation, 2003].

[15] Two out of three calcareous samples from unit IV (1149B 27R1 49–55 and 1149B 29R1 28–35) have similar $^{87}Sr/^{86}Sr$ (0.7076–0.7081, $^{143}Nd/^{144}Nd$ (0.51226–0.51231), $^{206}Pb/^{204}Pb$ (18.38–18.48), $^{207}Pb/^{204}Pb$ (15.53–15.54) and $^{208}Pb/^{204}Pb$ (38.14–38.30) isotopic ratios to the clay sample from unit III and may reflect the presence of clay in these samples (Figures 3 and 4 and Tables 2a–2c). According to point-counting

Table 2c. Measured and Initial Pb Isotope Data of ODP Site 1149 and 801 Samples[a]

Sample	Age, Ma	Pb	U	Th	$^{238}U/^{204}Pb$	$^{232}Th/^{238}U$	$^{206}Pb/^{204}Pb$	±2σ	$^{207}Pb/^{204}Pb$	±2σ	$^{208}Pb/^{204}Pb$	±2σ	$^{206}Pb/^{204}Pb_{in}$	$^{207}Pb/^{204}Pb_{in}$	$^{208}Pb/^{204}Pb_{in}$
							1149A								
1149A 4H2 140–150	5	25.0	1.51	9.26	3.87	6.32	18.624	(1)	15.612	(1)	38.730	(1)	18.621	15.612	38.724
1149A 10H3 140–150	10	20.9	1.34	6.27	4.11	4.82	18.589	(1)	15.615	(1)	38.715	(1)	18.583	15.614	38.705
1149A 14H2 140–150	19	25.8	1.63	8.82	4.04	5.59	18.619	(1)	15.613	(1)	38.732	(1)	18.603	15.612	38.702
1149A 20X1 140–150	44	52.0	2.79	25.13	3.43	9.31	18.610	(6)	15.624	(6)	38.785	(2)	18.586	15.623	38.715
							1149B								
1149B 6R1 38–42	47	5.3	2.24	1.37	27.36	0.63	19.046	(1)	15.634	(1)	38.639	(1)	18.846	15.625	38.599
1149B 11R1 19–22	70	4.8	1.78	1.80	23.65	1.05	19.006	(1)	15.636	(1)	38.730	(2)	18.748	15.624	38.644
1149B 12RCC 0–5	90	28.6	1.12	6.73	2.48	6.22	18.515	(1)	15.547	(1)	38.347	(2)	18.480	15.545	38.278
1149B 16R1 93–98	100	5.1	0.60	5.25	7.45	9.11	18.783	(1)	15.608	(1)	38.861	(1)	18.666	15.602	38.524
1149B 27R1 49–55	120	3.3	0.13	0.77	2.44	6.21	18.481	(2)	15.541	(2)	38.305	(5)	18.435	15.538	38.215
1149B 29R1 28–35	120	7.3	0.52	1.57	4.53	3.09	18.379	(1)	15.528	(8)	38.140	(2)	18.294	15.524	38.057
1149B 30R1 61–66	130	0.3	0.10	0.10	24.89	0.97	18.484	(4)	15.420	(4)	37.566	(9)	17.977	15.395	37.411
1149B 30R2 56–62	130	0.4	0.15	0.15	21.62	1.08	18.500	(3)	15.435	(2)	37.517	(5)	18.059	15.414	37.367
							1149C								
1149C 10R2 47–51	130	1.0	0.28	0.18	18.05	0.65	17.884	(2)	15.470	(2)	37.263	(4)	17.516	15.452	37.187
							1149D								
1149D 7R1 37–42	130	0.3	0.15	0.14	30.92	0.95	18.742	(3)	15.457	(2)	37.807	(6)	18.113	15.427	37.618
1149D 8R2 16–19	130	0.1[b]	0.05	-	51.39	-	20.029	(28)	15.569	(22)	37.677	(52)	18.982	15.518	
1149D 9R3 30–32	130	0.4	0.20	0.19	28.25	0.99	18.492	(3)	15.434	(3)	37.642	(7)	17.916	15.406	37.461
1149D 11R2 86–92	130	0.4	0.11	0.12	17.86	1.14	19.225	(5)	15.450	(4)	37.762	(9)	18.862	15.432	37.630
1149D 16R3 2–8	130	0.6	0.31	0.44	31.50	1.48	18.944	(3)	15.461	(2)	38.079	(5)	18.302	15.430	37.779
1149D 17R1 92–98	130	0.6	0.22	0.39	24.43	1.88	18.900	(3)	15.471	(2)	38.117	(5)	18.403	15.447	37.821
1149D 19R1 85–89	130	0.7	0.13	0.39	11.95	3.19	18.299	(3)	15.422	(2)	37.757	(5)	18.055	15.410	37.511
							801B								
801B 43R1 132–135	157	1.9	0.78	2.40	26.19	3.18	19.363	(2)	15.553	(1)	38.622	(3)	18.718	15.521	37.972
							801C								
801C 4R1 72–77	167	0.2	0.11	0.02	32.05	0.22	18.965	(4)	15.557	(4)	37.891	(9)	18.124	15.516	37.833
801C 15R7 31–34	167	1.1	0.48	0.21	26.47	0.46	18.725	(2)	15.483	(2)	37.495	(4)	18.030	15.448	37.393
801C 17R4 15–18	167	0.8	0.01	-	0.55	-	26.843	(95)	15.734	(55)	38.708	(136)	26.828	15.734	
801C 19R2 24–27	167	0.1	0.09	0.09	58.98	1.01	19.050	(5)	15.499	(4)	37.633	(9)	17.502	15.422	37.139
801C 34R1 93–96	167	0.7	0.79	0.25	67.91	0.33	19.436	(1)	15.518	(1)	37.456	(2)	17.653	15.430	37.271
801C 40R1 24–27	167	0.3	1.65	0.14	330.66	0.09	26.860	(5)	15.838	(3)	37.535	(6)	18.182	15.409	37.286
801C 44R3 23–26	167	0.3	1.47	0.21	283.78	0.15	23.699	(4)	15.788	(3)	37.644	(7)	16.251	15.421	37.299

[a] Initial isotope ratios use element concentration data from *Kelley et al.* [2003]. Internal errors refer to the last significant digit(s).The calculation of initial $^{207}Pb/^{204}Pb$ and $^{208}Pb/^{204}Pb$ is not affected by propagated errors from the U-Th-Pb concentration data. This is also the case for initial $^{206}Pb/^{204}Pb$ in most samples except for those with extreme U/Pb ratios, namely 1149D 8R2 16–19 (±0.021), 801C 19R2 24–27 (±0.031), 801C 34R1 93–96 (±0.035), 801C 40R1 24–27 (±0.173), 801C 44R3 23–26 (±0.148).

[b] Determined from Nd/Pb = 24 after *Rehkämper et al.* [1997].

Table 3. Site 1149 Sediment End-Members and Bulk Sediment Composition[a]

Site 1149 Sediments	Number of Analyses	Sr, ppm	$^{87}Sr/^{86}Sr$	Nd, ppm	$^{143}Nd/^{144}Nd$	Pb, ppm	$^{206}Pb/^{204}Pb$	$^{207}Pb/^{204}Pb$	$^{208}Pb/^{204}Pb$
Sediment End-Members by Lithology									
Upper clay (Unit I & II)	4	147	0.71088	72	0.51233	31	18.61	15.62	38.75
Izu ash[b]	29	165	0.70355	8	0.51308	4	18.36	15.51	38.19
Chert (Unit III)	2	33	0.71330	13	0.51228	5	19.03	15.64	38.68
Lower clay (Unit III)	1	161	0.71286	64	0.51229	29	18.52	15.55	38.35
Carbonate + lower clay	2	385	0.70776	15	0.51229	5	18.41	15.53	38.19
Carbonate[c]	1	302	0.70758	4	0.51229	0.3	18.84	15.62	38.65
Site 1149 Unit Averages, vol%									
Avg unit I and II; upper clays n = 4	43.9%	147	0.71088	72	0.51233	31	18.61	15.62	38.75
Avg unit III n = 3	24.4%	76	0.71300	30	0.51229	13	18.65	15.57	38.43
Avg unit IV n = 3	31.7%	333	0.70812	23	0.51241	5	18.53	15.56	38.41
Average 1149 sediment this study	100%	189	0.70954	46	0.51234	18	18.61	15.60	38.67
IZU sediment average[d]		110	0.70617	29	0.51252	7	18.92	15.65	38.92
Mariana sediment average[d]		161	0.70617	21	0.51252	6	18.92	15.65	38.92
GLOSS[d]		327	0.71730	27	0.51218	20	18.91	15.67	38.90

[a] Trace element concentrations from *Kelley et al.* [2003].
[b] Data from Schmidt et al. (manuscript in preparation, 2003).
[c] Data from *Hochstaedter et al.* [2001].
[d] Published average sediment input of the Izu and Mariana arc *Plank and Langmuir* [1998] are shown for comparison as well as globally subducted sediment (GLOSS). The sediment end-members of the Izu-Bonin Arc system refer to individual lithologies identified in the sediment column of the subducted oceanic plate at Site 1149. The corresponding lithological units are listed in parentheses. The isotopic compostion of sediment end-members uses concentration and isotopic data from Tables 2a, 2b, and 2c and represents the concentration weighted mean of the analyzed samples. Site 1149 Unit averages represent the concentration weighted mean of all analyzed samples occuring in a particular unit. The average 1149 sediment of this study represents the unit averages weighted to their volumetric abundance.

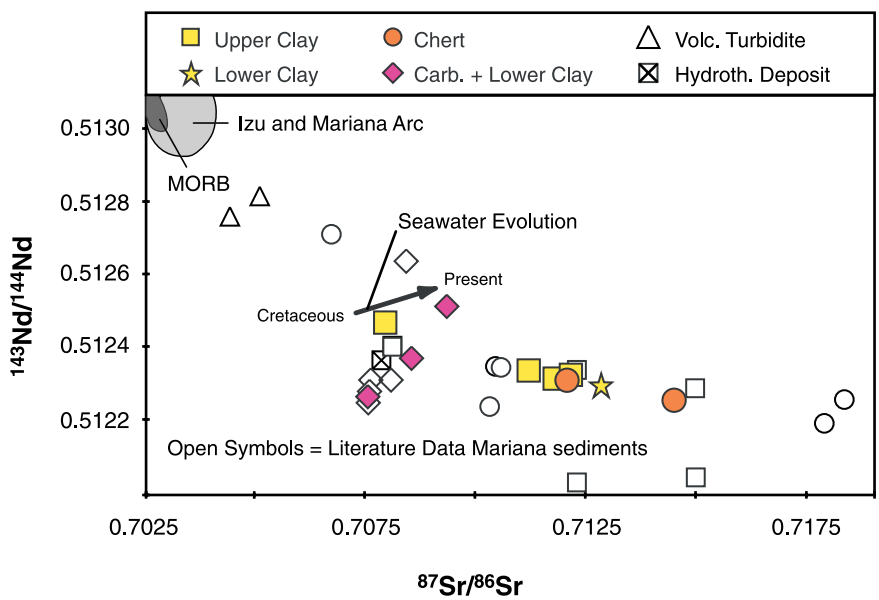

Figure 3. Sr-Nd isotope correlation diagram for Site 1149 sediments (filled symbols) along with literature data of sediment from Mariana arc (open symbols). The upper clays are from Unit I and II and the lower clays from unit III. Cherts come from unit III and carbonates from unit IV. Literature data are from *Lin* [1992], *Plank and Langmuir* [1998], *Pearce et al.* [1999], *Hochstaedter et al.* [2001]. Izu arc: Schmidt et al. (manuscript in preparation, 2003); Mariana arc: *Elliott et al.* [1997]; Pacific MORB: *Ito et al.* [1987] and *White et al.* [1987].

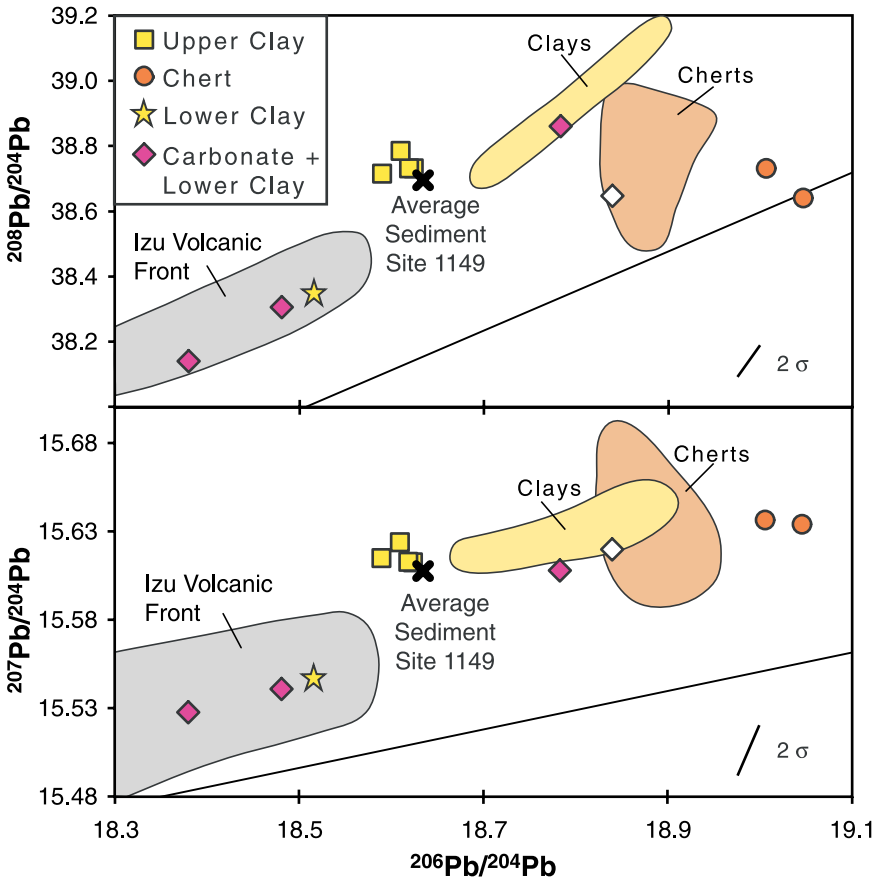

Figure 4. Pb isotope diagrams for Site 1149 sediments. Symbols as in Figure 3. Open symbols as well as yellow and orange fields are literature data of regional clays and cherts respectively [*Hochstaedter et al.*, 2001; *Pearce et al.*, 1999; *Plank and Langmuir*, 1998]. Fields for the Izu volcanic front from Schmidt et al. (manuscript in preparation, 2003).

analyses of smear slides [*Plank et al.*, 2000], all carbonates contain 5–35% clay. As is the case for the clay sample from unit III, the Pb isotopic composition of these clay-bearing calcareous samples overlaps with that of the recent Izu Volcanic Front rocks. The third calcareous sample (1149B 16R1 93–98) from unit IV is significantly more radiogenic in Sr, Nd and Pb isotopic composition ($^{87}Sr/^{86}Sr$ = 0.7094, $^{143}Nd/^{144}Nd$ = 0.51251, $^{206}Pb/^{204}Pb$ = 18.78; $^{207}Pb/^{204}Pb$ = 15.61, $^{208}Pb/^{204}Pb$ = 38.86) than the other two chalk samples (Figures 3 and 4 and Tables 2a–2c). This sample, which contains a noteworthy amount of radiolarians (15–35%) and some clay, lies on a mixing line between cherts and the clay-bearing carbonate samples from this study on the Sr-Nd and Pb-Pb isotope correlation diagrams (Figures 3 and 4). Since pure carbonate has very low Nd and Pb concentrations, similar to carbonate sample 195B-3-1 129–130 from *Hochstaedter et al.* [2001] with Nd of 3.9 ppm and Pb of 0.3 ppm (see Table 3), even small amounts of chert and clay can significantly alter the isotopic composition of these samples. Due to the high Sr content of carbonate, the $^{87}Sr/^{86}Sr$ ratio of the carbonates will be minimally affected by the addition of clay.

[16] In summary, the Sr-Nd isotope data of the sediments falls within the range of previous data from other ODP/DSDP Sites East of the Izu-Bonin-Mariana trench (Figure 3). The Pb isotope data of sediments in this study, however, show considerably greater variation than previously observed (Figure 4). Particularly noteworthy are (1) the less radiogenic Pb isotopic ratios of the lower (Unit III and IV) zeolite clay and clay-bearing carbonate as

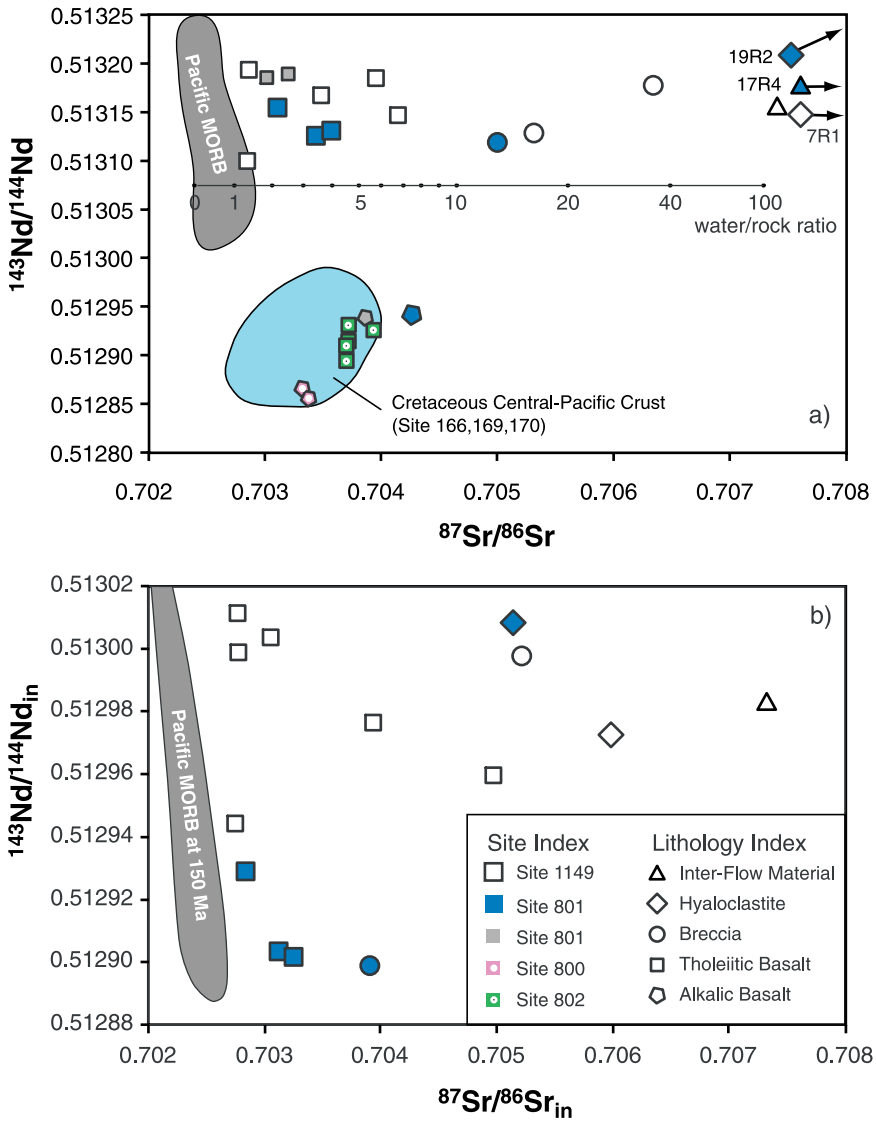

Figure 5. Measured (a) and initial (b) Sr-Nd isotope ratios of basaltic ocean crust from Site 1149 (open symbols) and Site 801 (blue symbols) analyzed during this study. All other symbols and the field for Cretaceous Central Pacific crust are literature data from Site 166, 169, 170, 800, 801 and 802 [*Castillo et al.*, 1992a; *Janney and Castillo*, 1996] with $^{143}Nd/^{144}Nd$ normalized to La Jolla of this paper. Pacific MORB fields after *Ito et al.* [1987] and *White et al.* [1987]. See text for details on water/rock ratio.

compared to the upper (Unit I and II) clays and (2) the overlap in the Pb isotopic composition of the lower clay and clay-bearing carbonate with the Izu Volcanic Front rocks.

2.2. Igneous Basement: Site 1149

[17] A total of five fresh to variably altered basalts, one inter-flow material sample, three breccias and one smectite bearing hyaloclastite from the igneous basement of Site 1149 were investigated. The samples span a wide range in $^{87}Sr/^{86}Sr$ = 0.7029–0.7115 and $^{206}Pb/^{204}Pb$ = 17.88–20.03, whereas $^{207}Pb/^{204}Pb$ = 15.42–15.57; $^{208}Pb/^{204}Pb$ = 37.26–38.12 and $^{143}Nd/^{144}Nd$ = 0.51310–0.51319 vary only slightly (Figures 5 and 6 and Tables 2a–2c). Initial Sr and Pb ($^{206}Pb/^{204}Pb$ primarily) show less considerable variation: $(^{87}Sr/^{86}Sr)_{in}$ = 0.7028–0.7073, $(^{143}Nd/^{144}Nd)_{in}$ = 0.51294–0.51301, $(^{206}Pb/^{204}Pb)_{in}$ = 17.52–18.98, $(^{207}Pb/^{204}Pb)_{in}$ = 15.40–15.52, $(^{208}Pb/^{204}Pb)_{in}$ = 37.19–37.82. All calcite-bearing samples namely breccias, veined basalt and inter-flow material,

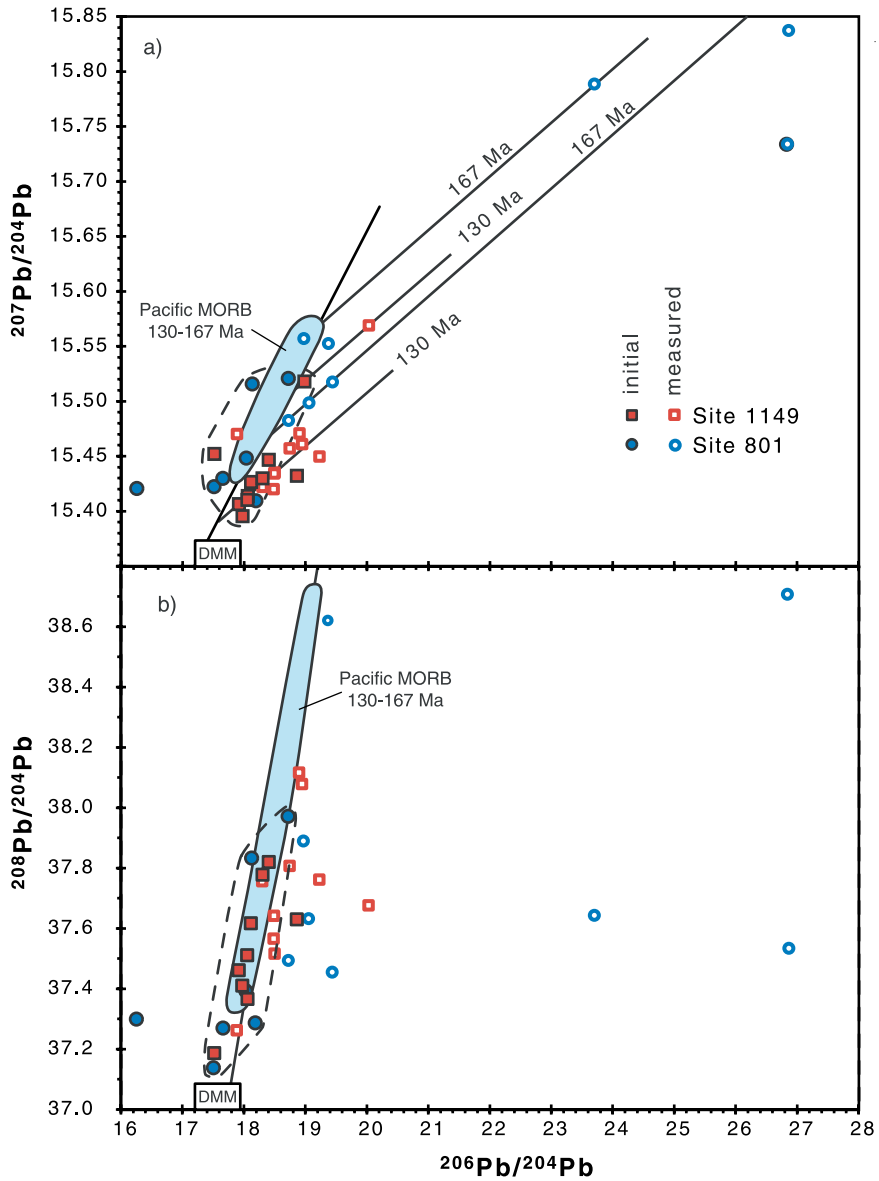

Figure 6. $^{206}Pb/^{204}Pb$ versus $^{207}Pb/^{204}Pb$ (a) and $^{206}Pb/^{204}Pb$ versus $^{208}Pb/^{204}Pb$ (b) isotope diagrams for Site 1149 and Site 801 basaltic ocean crust. The field for 130–170 Ma Pacific MORB was calculated using present-day Pacific MORB assuming $^{238}U/^{204}Pb = 5$ and $^{232}Th/^{238}U = 2.5$ for the MORB source after *White* [1993]. 130 Ma and 167 Ma reference isochrons are also shown. Dashed line encircles ~88% of the initial Pb isotope data.

have initial $^{87}Sr/^{86}Sr$ ratios (0.7030–0.7073) lower than seawater but are higher than the least radiogenic basalt with $(^{87}Sr/^{86}Sr)_{in} = 0.7027$. Altered basalt free of secondary calcite veins has initial $^{87}Sr/^{86}Sr$ ratios of up to 0.7039. On the uranogenic and thorogenic Pb isotope diagrams, the measured Pb isotope data extends from the field of Pacific MORB to the right of the Pacific MORB array (Figure 6). They do not overlap with any known fields of mantle-derived rocks and generally fall below literature data for altered Pacific MORB from other regions.

2.3. Igneous Basement: Site 801

[18] Four variably altered basalts, one sample from the upper hydrothermal unit, one hyaloclastite, one breccia and one inter-flow material sample were analyzed from Site 801 (Table 1). Compared to the igneous basement samples from Site 1149, the Site

801 samples extend to significantly more radiogenic $^{206}Pb/^{204}Pb$ (18.73–26.86) and $^{207}Pb/^{204}Pb$ (15.48–15.84) and to less radiogenic $^{143}Nd/^{144}Nd$ ratios (0.51294–0.51334, except hydrothermal sample 801C 4R1 72–77 with 0.51237 Table 2). If sample 801C 4R1 72–77 is excluded (discussed below), $^{87}Sr/^{86}Sr$ ratios (0.7031–0.7099) and $^{208}Pb/^{204}Pb$ (37.46–38.71) are similar to those observed for Site 1149 basement samples. Initial isotope ratios $(^{87}Sr/^{86}Sr)_{in}$ = 0.7028–0.7069 and $(^{143}Nd/^{144}Nd)_{in}$ = 0.51281–0.51301 (excluding sample 801C 4R1 72–77) display similar systematics as in Site 1149 (Figure 5). The range of age corrected Pb isotope data (excluding sample 801C 17R4 15–18), however, is broader for $(^{206}Pb/^{204}Pb)_{in}$ = 16.25–18.72 and $(^{207}Pb/^{204}Pb)_{in}$ = 15.41–15.52 than at Site 1149 but similar in $(^{208}Pb/^{204}Pb)_{in}$ = 37.14–37.97 (Figure 6). The extremely high initial ratios of sample 801C 17R4 15–18 ($(^{206}Pb/^{204}Pb)_{in}$ = 26.83 and $(^{207}Pb/^{204}Pb)_{in}$ = 15.73) most likely represents an undercorrection for the effects of radioactive decay of U, suggesting the time integrated U was considerably higher than the measured U of 0.01 ppm.

[19] The highest $^{87}Sr/^{86}Sr$ ratios (0.7099 and 0.7257) occur in the smectite-bearing inter-flow material sample 801C 17R4 15–18 and hyaloclastite sample 801C 19R2 24–27, which also have the highest $^{87}Rb/^{86}Sr$ ratios of 10.5 and 2 that lead to initial $^{87}Sr/^{86}Sr$ of 0.7008 and 0.7051 respectively. The extremely low initial $^{87}Sr/^{86}Sr$ of sample 801C 17R4 15–18 represents an overcorrection for radioactive decay of ^{87}Rb, indicating that the present $^{87}Rb/^{86}Sr$ ratio (10.5) is higher than the time-integrated Rb/Sr ratio. $^{87}Sr/^{86}Sr$ in all inter-flow material samples is more radiogenic than in fresh MORB. The Nd isotopic ratios of the smectite-bearing samples ($^{143}Nd/^{144}Nd$ = 0.51319–0.51334) are slightly higher than those of the pure basaltic samples ($^{143}Nd/^{144}Nd$ = 0.51294–0.51315), whereas the calcite-bearing inter-flow breccia 801C 40R1 24–27 has similar Nd isotopic composition as the associated basalts. The inter-flow material and hyaloclastite are thus significantly more radiogenic in $^{143}Nd/^{144}Nd$ than layer 1 sediments at Site 1149. The hydrothermal sample 801C 4R1 72–77 is very close to Mesozoic seawater in both $^{87}Sr/^{86}Sr$ = 0.7078 and $^{143}Nd/^{144}Nd$ = 0.51237 (Figure 3).

[20] The tholeiitic basalts of Site 801 have similar Sr-Nd isotopic compositions ($^{87}Sr/^{86}Sr$ = 0.7031–0.7036, $^{143}Nd/^{144}Nd$ = 0.51313–0.51315) to those from Site 1149 ($^{87}Sr/^{86}Sr$ = 0.7028–0.7042, $^{143}Nd/^{144}Nd$ = 0.51310–0.51319). In this respect the low $^{143}Nd/^{144}Nd$ = 0.51294 of an aphyric alkali basalt (801B 43R1 132–135) at this Site is somewhat exceptional but similar basalts are also described from Site 800 and 802 [*Castillo et al.*, 1992a]. All Site 801 basalt samples have higher $^{207}Pb/^{204}Pb$ (15.48–15.79) than at Site 1149 ($^{207}Pb/^{204}Pb$ = 15.42–15.47). On the uranogenic and thorogenic Pb isotope diagrams (Figure 6), the samples from Site 801 extend from the Pacific MORB field or NHRL significantly to the right as is also observed for the Site 1149 basalts. Extremely radiogenic $^{206}Pb/^{204}Pb$ (23.70–26.86) and $^{207}Pb/^{204}Pb$ (15.79–15.84) ratios are present in an altered basalt (801C 44R3 23–26), a calcite-rich breccia (801C 40R1 24–27) and calcite-smectite-bearing inter-flow material sample (801C 17R4 15–18). Such intriguing $^{206}Pb/^{204}Pb$-$^{207}Pb/^{204}Pb$ ratios are the most extreme ever measured in altered MORB, even higher than found in Atlantic MORB of similar age with $^{206}Pb/^{204}Pb$ and $^{207}Pb/^{204}Pb$ extending to 20.75 and 15.72 respectively [*Hoernle*, 1998]. The $^{208}Pb/^{204}Pb$, $^{87}Sr/^{86}Sr$ and $^{143}Nd/^{144}Nd$ ratios of the samples with anomalously high $^{206}Pb/^{204}Pb$ and $^{207}Pb/^{204}Pb$, however, are similar to the other igneous basement samples from Site 1149 and 801.

3. Discussion

3.1. Origin of Sr-Nd-Pb Isotopic Compositions in the Mesozoic Upper Ocean Crust: Evolution on the Seafloor

3.1.1. Sediments

[21] On the basis of mineralogy and Sr-Nd-Pb isotopic composition, five sediment end-members can be identified in the sediment column of Site 1149: (1) upper clay from Units I and II, (2) volcanic ash from Unit I, (3) chert from Unit III, (4) lower clay from lower Unit III and Unit IV,

Table 4. Sr Isotope Data for Clays and Cherts, Except Sample 1149A 10H3 140–150 From Unit I Containing Volcanic Ash[a]

Sample Number	Unit/Lithology	Calculated Age	$^{87}Sr/^{86}Sr_m$	$^{87}Sr/^{86}Sr_{in}$
1149A 4H2 140–150	I/clay	5	0.711255	0.71110
1149A 14H2 140–150	II/clay	19	0.711782	0.71111
1149A 20X1 140–150	II/clay	44	0.712182	0.71111
1149B 6R1 38–42	III/chert	47	0.712081	0.71110
1149B 11R1 19–22	III/chert	147	0.714509	0.71111
1149B 12RCC 0–5	III/clay	90	0.712861	0.71110

[a] Assuming an Late Pliocene age of 5 Ma for the uppermost clay sample (1149A 4H2) and assumming that the other clay and chert samples have the same initial $^{87}Sr/^{86}Sr$ as this sample, ages of the different units are calculated. With the exception of chert sample 1149B 11R1, the ages agree reasonably well with the stratigraphy showing that the differences in measured $^{87}Sr/^{86}Sr$ may primarily reflect in situ decay of ^{87}Rb after deposition instead of differences in source composition.

and (5) carbonate from Unit IV (see Table 3). The isotopic composition of carbonate will reflect that of the seawater from which it precipitated, if it does not contain impurities. The isotopic composition of clay and chert, on the other hand, will reflect that of its continental sources. The main source of the volcanic ash is the Izu Arc.

[22] Sr concentration and isotopic composition vary considerably in the sediments (Table 3). Average chert has the lowest Sr concentrations (as low as 33 ppm), carbonate the highest (up to 483 ppm), and clay and ash intermediate concentrations (concentration data for the samples discussed in this manuscript are from *Kelley et al.* [2003]. Average Izu volcanic ash from Site 782 (Schmidt et al., manuscript in preparation, 2003) has the lowest $^{87}Sr/^{86}Sr$ (0.7035); carbonate has intermediate $^{87}Sr/^{86}Sr$ similar to seawater; whereas clay and chert have high, continental-type $^{87}Sr/^{86}Sr$ (0.7113–0.7145, excluding clay sample with ash). Excluding the clay sample with volcanic ash (1149A 10H3 140–150), there is a general increase in the $^{87}Sr/^{86}Sr$ ratio of the clays and cherts from Unit I to Unit II to Unit III (Figure 3). Considering the large $^{87}Rb/^{86}Sr$ ratios (1.4–1.7; Tables 2a–2c) of the clays and cherts, the increase in the measured $^{87}Sr/^{86}Sr$ isotope ratios with depth in the core may at least partially reflect in situ decay (Table 4). It is interesting to note that if we assume an age of 5 Ma for the uppermost clay sample and then assume that all other samples have the same initial $^{87}Sr/^{86}Sr$ to this sample, we calculate reasonable ages which agree with the stratigraphy for all samples except chert 1149B 11R1 (Table 4). In conclusion, considering the large $^{87}Rb/^{86}Sr$ ratios and the uncertainty in the depositional age of the sediments, it is not clear if the differences in $^{87}Sr/^{86}Sr$ reflect differences in in situ decay or source variations.

[23] Nd concentration is low in the ashes, cherts and carbonates but highly variable in the clays, reaching concentrations in excess of 200 ppm [*Kelley et al.*, 2003], possibly reflecting the presence of Mn deposits. The Nd isotopic composition of the clays, cherts and carbonates are surprisingly uniform at ~0.5123. The ash however has significantly higher $^{143}Nd/^{144}Nd$ of ~0.5131. Since $^{147}Sm/^{144}Nd$ ratios are relatively low (0.11–0.14; Tables 2a–2c), initial values do not deviate substantially from the measured values.

[24] Although the Sr and Nd isotopic data fall within the range of previous sediment analyses from the region, the Pb isotopic composition shows considerably larger variation. Pure carbonate has very low Pb concentrations, reflecting the low Pb concentrations in seawater. The Pb concentration of carbonte is similar to that measured in chalk sample 195B-3-1 129–130 (0.3 ppm; [*Hochstaedter et al.*, 2001]). Volcanic ash and chert have intermediate concentrations of Pb, whereas clay has very high concentrations [*Kelley et al.*, 2003]. The most radiogenic Pb isotopic composition is observed in the cherts (Figure 4). Chalk sample 195B-3-1 129–130 also has radiogenic Pb but this could reflect small amounts of chert in this sample. The four uppermost clay samples have a surprisingly uniform and intermediate Pb isotopic composition. The lower clay, carbonate with clay samples from the base of the sediment column and

Izu volcanic ash have the least radiogenic Pb isotopic compositions. The 20–25% clay contents of the carbonates as is evident from the elevated Nd and Pb concentrations (compare concentrations of "carbonate with clay" with carbonate and lower clay in Table 3), will dominate both the Nd and Pb isotopic compositions. The similarity in average Pb isotopic composition of the Izu Volcanic Front ash ($^{206}Pb/^{204}Pb$ = 18.41, $^{207}Pb/^{204}Pb$ = 15.52 and $^{208}Pb/^{204}Pb$ = 38.25) and that of the lowermost two carbonate with clay) samples at Site 1149 (18.43, 15.53, 38.22) is particularly striking.

[25] As is observed for the different sediment types, the lithostratigraphic units from Site 1149 (Figure 2) also display differences in isotopic composition (Table 3) primarily reflecting the main sediment components in these units. The uppermost unit consists primarily of clay and volcanic ash from the Izu Arc. As is illustrated by comparing sample 1149A 10H3 140–150 with 1149A 4H2 140–150 (Tables 2a–2c), addition of ash to the clay causes a significant decrease in the Sr, only a small increase in the Nd, and a small decrease in the Pb isotope ratios. Considering that the volume of ash is small and that the clay can have up to an order of magnitude higher Nd and Pb concentrations although similar Sr concentrations [*Kelley et al.*, 2003] the ash will have little effect on the bulk sediment composition of Unit I or Site 1149 except to decrease the Sr isotopic composition. The Unit II clays (1149A 14H2 140–150, 1149B 20X1 140–150) have slightly more radiogenic Sr but the Nd and Pb isotopic composition are identical to the ash-free clay from Unit I (1149A 4H2 140–150). As noted above and in Table 3, the slightly more radiogenic Sr of the lower unit is likely to reflect radiogenic ingrowth of ^{87}Sr.

[26] Unit III is dominated by cherts which extend to still higher $^{87}Sr/^{86}Sr$ than the upper clays. The $^{143}Nd/^{144}Nd$, $^{207}Pb/^{204}Pb$ and $^{208}Pb/^{204}Pb$ of the cherts are very similar to those of the clays ± ash but has significantly higher $^{206}Pb/^{204}Pb$. The high $^{206}Pb/^{204}Pb$ ratio is consistent with high $^{238}U/^{204}Pb$ (μ) of the cherts (24–27) compared to the clays (3–4). The initial Pb isotope ratios of the upper clays and cherts are nearly identical, indicating derivation of the Pb from a common continental source (Tables 2a–2c). Clay sample 1149B 12RCC 0–5 from the lower part of unit III (referred to as the lower clay) has distinctly less radiogenic Pb isotopic compositions, which remains distinct even if the initial ratios are compared to those of the upper clays, indicating a change in the source of the clay during the Late Cretaceous to Early Tertiary during which Unit III was deposited.

[27] Unit IV is dominated by carbonate material containing clay and chert. The carbonates of this unit have the lowest $^{87}Sr/^{86}Sr$ of any unit, which is similar to or slightly higher than Cretaceous to Holocene seawater. Due to the low Nd and Pb contents of carbonate, the Nd and Pb isotopic compositions of the Unit IV samples are dominated by clay and chert within the carbonate material. The Pb isotopic composition of the radiolarite-bearing carbonate (1149B 16R1) at the top of Unit IV is consistent with the presence of chert and smaller amounts of clay in this sample. The expected two component mixing relationship is more clearly evident when initial Pb isotopic ratios are considered. The two carbonate samples (1149B 30R1 and 30R2) which contain clay have the least radiogenic Pb isotopic compositions found within the sediment column at Site 1149, confirming a change in the source of the clay in the early Tertiary.

[28] In summary, the compositions of the sediments at Site 1149 are primarily dominated by the upper clays in Units I and II, cherts and lower clays in Unit III, and lower clays in Unit IV. The Pb isotopic composition of the lower clays is surprisingly similar to the composition of the Izu Volcanic Front rocks. Our estimate of the bulk sediment composition at Site 1149 (see Table 3) produces a $^{87}Sr/^{86}Sr$ value (0.7094) slightly higher than Cretaceous to Holocene seawater [*Ingram*, 1995; *Elderfield*, 1986], a $^{143}Nd/^{144}Nd$ ratio (0.51235) similar to seawater and Pb isotopic composition very similar to the upper clays, which dominate the Pb due to their high Pb concentrations. We note that our Izu sediment average produces more radiogenic Sr and Nd isotope ratios but less radiogenic Pb isotope ratios than the Izu sediment average of *Plank and Langmuir* [1998] (see Table 3), which was based primarily on the upper-

most sediments in front of the Mariana trench. We also note that our Izu average has considerably less radiogenic Sr and Pb than the composition of average global subducted sediment (GLOSS, [*Plank and Langmuir*, 1998]), possibly reflecting a somewhat unique source for the lower Izu clays.

3.1.2. Basaltic Ocean Crust

[29] The Sr-Nd-Pb isotopic composition of the basaltic ocean crust is primarily controlled by (1) the mantle source from which the melts are extracted, (2) the type and degree of seafloor alteration, and (3) the age of the crust. Since both Sm and Nd are generally considered to be relatively immobile during seafloor alteration, the initial Nd isotopic composition of the igneous crust will most closely reflect that of its source. Both Rb and Sr are fluid mobile elements. Coupled with the relatively high Sr content in seawater of ~7.7 ppm and the radiogenic Sr composition of seawater [e.g., *Faure*, 1986], seawater alteration of basaltic crust almost always causes an increase in the $^{87}Sr/^{86}Sr$ ratio. The relatively short half-lives of ^{235}U ($t_{1/2} = 0.71 \times 10^9$yr); ^{238}U ($t_{1/2} = 4.47 \times 10^9$yr) and ^{232}Th ($t_{1/2} = 14 \times 10^9$yr) in conjunction with the mobility of U (when oxidized to U^{+VI}) and Pb during hydrothermal alteration can cause significant changes of Pb isotope systematics in Cretaceous samples [e.g., *Hauff et al.*, 2000a, 2000b; *Hoernle*, 1998]. Hydrothermal activity generally does not affect the uppermost portions of the igneous crust (presently accessible through drilling) unless a later magmatic event has occurred, associated with hot spot volcanism. Variations in the $^{238}U/^{204}Pb$ or μ ratio, resulting from the high mobility of U, can have a large effect on the $^{206}Pb/^{204}Pb$ ratio over time (tens to hundreds of millions of years). Due to the low abundance of ^{235}U ($^{238}U/^{235}U = 137.88$) presently on the Earth, the $^{207}Pb/^{204}Pb$ ratio will only be affected when substantial U relative to Pb enrichments occur as a result of seafloor alteration. Since Th is also highly immobile, the Th/Pb ratio will generally not be affected during low temperature alteration within the uppermost parts of the igneous crust. Therefore the initial $^{208}Pb/^{204}Pb$ isotope ratios should also reflect those of the source. In conclusion, the initial $^{143}Nd/^{144}Nd$, $^{207}Pb/^{204}Pb$ (when μ is low) and $^{208}Pb/^{204}Pb$ isotopic ratios should reflect those of the mantle source(s) of the basalts, yet $^{87}Sr/^{86}Sr$ and $^{206}Pb/^{204}Pb$ are sensitive to seafloor alteration processes, particularly in aged (e.g., Mesozoic) ocean crust.

[30] During ODP Leg 185, 133 m of 130 Ma tholeiitic basalts were drilled at Site 1149 and 474 m of both alkalic and tholeiitic basalts were drilled at Site 801 during ODP Leg 129 and Leg 185. The tholeiitic basalts from Site 1149 have relatively uniform $^{143}Nd/^{144}Nd$ (0.51310–0.51319), similar to basalts from the nearby basement Hole at Site 197 [*Janney and Castillo*, 1997]. The tholeiitic basalts from Site 801C have $^{143}Nd/^{144}Nd$ (0.51313–0.51315, except sample 801 19R2 with 0.51334). The Nd isotope data are consistent with derivation from depleted upper mantle: the source of normal mid ocean ridge basalts (N-MORB), and for the most part overlap the range previously observed at Site 801 [*Castillo et al.*, 1992a] (Figure 5a). Alkali basalt sample 801B 43R1 132–135A, however, has a more enriched isotopic composition, e.g., lower $^{143}Nd/^{144}Nd$ (0.51294), indicating derivation from an ocean island basalt (OIB)-type source.

[31] Previous geochemical studies of the igneous basement in front of the Marianas also show that the ocean floor is compositionally heterogeneous consisting of basalts with isotopically enriched and depleted mantle affinities [*Castillo et al.*, 1992a]. The basalts from ODP Leg 129 Sites 800 (126 Ma, [*Pringle*, 1992]) and 802 (111 Ma, [*Pringle*, 1992]) display exclusively enriched, OIB-type isotopic signatures and have much younger ages than the Jurassic (167 Ma) oceanic crust in this region. Both enriched and depleted basalts occur at Site 801. The enriched, OIB-type compositions are related to 157 Ma alkali basalts erupted on, and sills intruded into the 167 Ma tholeiitic basalts. In summary, multiple alkalic igneous events affected large portions of the Jurassic ocean floor east of the Marianas after its formation. The igneous activity is most likely related to the formation of the Magellan seamounts (Site 800 and 801) and the Ontong Java plateau (Site 802). Both of these enriched volcanic provinces are believed to be associated with mantle plumes [*Pringle*, 1992].

[32] Although samples within the tholeiitic basement have very similar $^{143}Nd/^{144}Nd$ ratios, the $^{87}Sr/^{86}Sr$ ratios show extremely large variation from 0.7029 to 0.7257 (Figure 5a). Nevertheless, the three samples with the highest $^{87}Sr/^{86}Sr$ ratios (hyaloclastite, breccia and inter-flow material) also have extremely high $^{87}Rb/^{86}Sr$ ratios of 2.0–10.5, whereas all other basement samples have $^{87}Rb/^{86}Sr < 0.5$. The initial $^{87}Sr/^{86}Sr$ ratios of the hyaloclastite and breccia samples fall within the range of other basement samples, whereas the initial $^{87}Sr/^{86}Sr$ ratio for inter-flow material sample 801C 17R4 15–18 of 0.7008 represents a clear over-correction for ^{87}Rb decay. If we assume the initial $^{87}Sr/^{86}Sr$ ratio of this sample to be 0.7024 (least radiogenic $^{87}Sr/^{86}Sr$ found at Site 801C; [*Castillo et al.*, 1992a, 1992b], then ca. 157 Ma are needed to generate a $^{87}Sr/^{86}Sr$ of 0.7257 with $^{87}Rb/^{86}Sr$ of 10.5. Therefore the anomalously high Rb enrichment of this inter-flow material may have occurred 10 Ma after the ocean crust formed, in conjunction with later OIB-type magmatism at 157 Ma. Inter-flow material sample 1149D 8R2 16–19, containing primarily carbonate, has an initial $^{87}Sr/^{86}Sr$ ratio of 0.7073, consistent with derivation of the carbonate from Late Cretaceous (130 Ma) seawater at the time the ocean crust at Site 1149 was formed. The initial $^{87}Sr/^{86}Sr$ ratios (Figure 5b) of the crust increase from the lavas (0.7027–39) to breccias (0.7035–52) to hyaloclastites (0.7051–60). The increase in $^{87}Sr/^{86}Sr$ ratio with decreasing size of basaltic fragments could result from increasing water/rock ratios for the lavas (1–7; assuming an unaltered initial $^{87}Sr/^{86}Sr$ ratio of 0.7024) to the breccias (7–20) to the hyaloclastites (20–30). Devitrification of basaltic glass is also likely to play a major role in the increase of $^{87}Sr/^{86}Sr$ in hyaloclastites. These water/rock ratios undoubtedly reflect maximum values, since seawater Sr has also clearly been added to these samples through precipitation of phases such as carbonate.

[33] Basaltic samples (lavas, breccias and hyaloclastites) from Site 1149 and 801 exhibit a wide range in $^{206}Pb/^{204}Pb$ (17.9–23.7) and μ (0.5 to 331; Tables 2a–2c) but have relatively uniform $^{207}Pb/^{204}Pb$ (except two samples) and $^{208}Pb/^{204}Pb$ (Figure 6). Since fresh MORB glasses generally posses μ-values of 10 or lower [*White*, 1993], the higher observed μ (12–331 for all but one sample) must have a secondary origin, most likely through addition of seawater derived U to the altered basalt. This mechanism would explain the large range in $^{206}Pb/^{204}Pb$ and of $^{207}Pb/^{204}Pb$ (in samples with extremely high μ) through radiogenic ingrowth. Interestingly, the initial Pb isotope ratios for most samples plot within or very close to the field for 130–170 Ma Pacific MORB on both Pb isotope diagrams (Figure 6). Therefore the μ of most samples must have been increased shortly (probably within 10 Ma) after formation of the crust. At Site 801, the change in μ may be related to later (occurring at ~157 Ma) igneous activity associated with the formation of the Magellan seamounts. Multiple alteration events, however, may have also occurred. While Rb-Sr systematics in sample 801C 17R4 15–18 are compatible with Rb enrichment ~10 Ma after ocean crust formation (see above), the very radiogenic $^{206}Pb/^{204}Pb$ of 26 requires time integrated μ's of at least 360. Instead the extremely low μ of 1 at present suggests recent U leaching, the mechanism of which remains unclear.

[34] Since no later igneous activity occurred near Site 1149, the change in μ is likely to have been increased near the spreading axis, as a result of increased circulation of crustal fluids in the uppermost ocean crust. These relations are illustrated by 130 Ma and 167 Ma reference isochrons shown on the $^{206}Pb/^{204}Pb$ versus $^{207}Pb/^{204}Pb$ isotope diagram (Figure 6a). These reference isochrons indicate that the measured $^{206}Pb/^{204}Pb$ and $^{207}Pb/^{204}Pb$ ratios (with the exception of inter-flow material sample 801C 17R4 15–18) could have been generated by radiogenic ingrowth. The estimated range in initial Pb isotopic composition for tholeiitic basalts at Site 801C ($^{206}Pb/^{204}Pb_i$ = 17.5–18.2; $^{207}Pb/^{204}Pb_i$ = 15.41–15.45; $^{208}Pb/^{204}Pb_i$ = 37.1–37.4) and Site 1149 ($^{206}Pb/^{204}Pb_i$ = 17.5–18.3; $^{207}Pb/^{204}Pb_i$ = 15.41–15.45; $^{208}Pb/^{204}Pb_i$ = 37.2–37.8), excluding basalt 1149D 11R2 86–92, overlaps with the unradiogenic end of Quaternary Pacific MORB (corrected for in situ decay in the source to 130–167 Ma) but also extends to slightly more depleted compositions (Figures 6a and 6b). In conclusion the initial Pb isotope data for Sites 1149 and 801

Table 5. Average Sr-Nd-Pb Isotopic Composition of the Upper Igneous Crust Site 1149 (n = 10) and 801 (n = 8)

Weighted to vol. and conc.[a]		vol%	Sr	$^{87}Sr/^{86}Sr$	Nd	$^{143}Nd/^{144}Nd$	Pb	$^{206}Pb/^{204}Pb$	$^{207}Pb/^{204}Pb$	$^{208}Pb/^{204}Pb$
					Site 1149					
Minimally altered basalt	n = 3	60%	145	0.703276	13.4	0.513144	0.75	18.30	15.45	37.63
Altered tholeiites	n = 4	30%	119	0.704792	9.6	0.513163	0.37	18.68	15.44	37.62
Veins and interflow material	n = 3	10%	115	0.706611	2.9	0.513148	0.31	18.92	15.47	37.99
Avg 1149 ig crust		100%	134	0.703967	11.2	0.513149	0.60	18.40	15.45	37.65
					Site 801					
Alkali basalt	n = 1	14%	350	0.704259	24.9	0.512941	1.92	19.36	15.55	38.62
Tholeiites	n = 4	80%	81	0.704229	7.5	0.513133	0.55	19.00	15.50	37.53
Veins and interflow material	n = 3	6%	94	0.706628	8.6	0.513136	0.50	26.11	15.77	38.19
Avg 801 ig crust		100%	119	0.704354	10.0	0.513066	0.74	19.42	15.53	37.95
Weighted to conc.[b]			Sr	$^{87}Sr/^{86}Sr$	Nd	$^{143}Nd/^{144}Nd$	Pb	$^{206}Pb/^{204}Pb$	$^{207}Pb/^{204}Pb$	$^{208}Pb/^{204}Pb$
					Site 1149					
Avg 1149 ig crust	n = 10		125	0.704769	9.4	0.513153	0.47	18.54	15.45	37.70
Min 1149 ig crust			50	0.702876	1.4	0.513100	0.06	17.88	15.42	37.26
Max 1149 ig crust			179	0.711516	15.9	0.513192	0.97	20.03	15.57	38.12
					Site 801					
Avg 801 ig crust	n = 8		119	0.704947	10.1	0.513075	0.70	21.02	15.59	38.08
Min 801 ig crust			2	0.703111	0.5	0.512369	0.10	18.73	15.48	37.46
Max 801 ig crust			350	0.725724	24.9	0.513340	1.92	26.86	15.84	38.71

[a] Weighted to volumetric abundance of lithologies (minimally basalt, altered basalt, interflow material etc) and concentrations.
[b] Average of all analyzed samples weighted to concentrations.

indicate that the source for Mesozoic Pacific MORB was roughly similar in the past and has evolved primarily through in situ radioactive decay over the last ~170 Ma. Some samples, however, appear to have undergone a more complex alteration history. For example, sample 801C 44R3 23–26 with $^{206}Pb/^{204}Pb_i = 16.25$ and $\mu = 284$ has been clearly over-corrected for radiogenic ingrowth of $^{206}Pb/^{204}Pb$, probably reflecting a later increase in μ. Sample 1149D 11R2 86–92 on the other hand has slightly elevated $^{206}Pb/^{204}Pb_i$ for its $^{207}Pb/^{204}Pb_i$ and $^{208}Pb/^{204}Pb_i$ possibly refelcting a relatively recent decrease in μ.

[35] The hydrothermal unit between the alkali basalts and tholeiitic basalts at Site 801 is presumably related to younger intraplate volcanism at 157 Ma. The unusually low $^{143}Nd/^{144}Nd$ ratio (0.51237) of sample 801C 4R1 72–77 from this unit is the least radiogenic found in any of our basement samples but falls within the restricted range of the sediments (excluding the volcanic ash; see Tables 2a–2c). The Nd isotopic composition suggests a sedimentary origin, most likely from hydrothermally-altered sediments deposited on the tholeiitic portion of the ocean crust between 157 and 167 Ma. The initial $^{87}Sr/^{86}Sr$ (0.7069) is similar to that found in Late Jurassic seawater. The Pb isotopes in contrast are quite similar to the low temperature altered basement samples (in particular the $^{208}Pb/^{204}Pb$ ratio), suggesting that the Pb, which is highly mobile in hydrothermal fluids, is primarily derived from the underlying tholeiitic ocean crust.

[36] The upper basaltic ocean crust at Sites 1149 and 801 has similar average Sr and Nd concentrations and isotopic composition (Table 5). The elevated $^{87}Sr/^{86}Sr$ at of 0.7040 at Site 1149 and 0.7044 at Site 801 clearly reflects the effect of low temperature seawater alteration on the oceanic crust: (1) increase in $^{87}Sr/^{86}Sr$ through addition of seawater Sr, and (2) increase in $^{87}Rb/^{86}Sr$ through preferential addition of Rb in comparison to Sr. The slightly lower average $^{143}Nd/^{144}Nd$ ratio of 0.513066 at Site 801 versus 0.513149 at Site 1149 results from the presence of younger alkalic volcanism at Site 801. The average $^{206}Pb/^{204}Pb$, $^{207}Pb/^{204}Pb$ and $^{208}Pb/^{204}Pb$ isotope ratios on the other hand show larger differences between the two

Sites with Site 1149 having lower $^{206}Pb/^{204}Pb$ (18.40), $^{207}Pb/^{204}Pb$ (15.45), $^{208}Pb/^{204}Pb$ (37.65) compared to Site 801 with $^{206}Pb/^{204}Pb$ (19.42), $^{207}Pb/^{204}Pb$ (15.53) and $^{208}Pb/^{204}Pb$ (37.95). In addition to the presence of alkali basalts, the more radiogenic average $^{206}Pb/^{204}Pb$ at Site 801 is also controlled by the much higher average μ at this Site (103, Tables 2a-2c) as compared to (23) at Site 1149 and thus is likely to result from radiogenic ingrowth. The higher μ's may be related to later igneous activity associated with the Magellan Seamount track, reflecting increased addition of U by fluids circulating within the crust.

3.2. Recycling at Subduction Zones: Relation Between Input and Output

[37] A fundamental question pertaining to the material fluxes through subduction zones is to what extent the output is influenced by the input. Several experimental studies [e.g., *Brenan et al.*, 1995a, 1995b; *Kosigo et al.*, 1997; *You et al.*, 1996] and geochemical investigations of island arcs [e.g., *Class et al.*, 2000; *Elliott et al.*, 1997; *Ishikawa and Nakamura*, 1994; *Morris et al.*, 1990; *Plank and Langmuir*, 1993; *Rüpke et al.*, 2002; *Vroon et al.*, 1995] reveal a link between subduction input (subducting slab including sediments, igneous oceanic crust and upper lithospheric mantle, possibly as serpentinite) and volcanic output.

3.2.1. Izu Arc

[38] There are several advantages of ODP Site 1149 in addressing material fluxes at subduction zones. First, drilling immediately east of the Izu trench has recovered the most complete upper section (543 m = 410 m of sediments and 133 m of igneous crust) of the oceanic crust entering the Izu subduction zone. Second, the direction of plate convergence is roughly parallel to the magnetic lineations of the Pacific Plate and thus the subducting crust beneath the Izu Arc is approximately of similar age to the ocean crust sampled in front of the trench (Figure 1). Third, seismic data [*Abrams*, 2002] show that the lithologies recovered from ODP Site 1149 extend along the strike of the arc and therefore are representative of the sediments subducting along the entire length of the Izu arc. Fourth, the Eocene through Holocene subduction output has been characterized in detail both laterally and spatially in the Izu Arc [e.g., *Taylor and Nesbitt*, 1998; *Hochstaedter et al.*, 2001; Schmidt et al., manuscript in preparation, 2003]. These circumstances in conjunction with the Sr-Nd-Pb isotope data presented here from the input allow us to explore the relationship between arc input and output in more detail. To avoid interlaboratory bias in isotopic composition, we use the data set for the Izu arc output from Schmidt et al. (manuscript in preparation, 2003). We note that this data set is very similar to that of [e.g., *Hochstaedter et al.*, 2001; *Taylor and Nesbitt*, 1998], but the Schmidt et al. (manuscript in preparation, 2003) data set shows better linear correlations in Pb isotope diagrams.

[39] The Izu Volcanic Front rocks have radiogenic $^{143}Nd/^{144}Nd$ (0.51307–0.51311, average = 0.51308, Table 3) and $^{87}Sr/^{86}Sr$ of 0.7033–0.7037 (Schmidt et al., manuscript in preparation, 2003). The $^{87}Sr/^{86}Sr$ of the Izu Volcanic Front is more radiogenic than the Indian MORB-type mantle wedge that is present beneath the arc and therefore requires a contribution from the subducting slab: seawater-altered oceanic crust and/or overlying sediments. The $^{143}Nd/^{144}Nd$ ratios of the Izu Volcanic Front on the other hand are generally less radiogenic than in the igneous ocean crust at Site 1149 (0.51313–19, except one sample with 0.51310, average = 0.51315, Table 5). Since the tholeiitic samples from Site 801 show a similar range in $^{143}Nd/^{144}Nd$ (0.51313–20, with one sample having 0.5133), $^{143}Nd/^{144}Nd$ ratios greater than 0.51313 may be representative of the Pacific oceanic crust in this region. If this is the case, then the primary source of the Nd in the Izu Volcanic Front rocks is likely to be the mantle wedge with a composition similar to Indian MORB based on studies of rear arc and back arc volcanic rocks [*Hickey-Vargas*, 1991; *Hickey-Vargas*, 1998; *Pearce et al.*, 1999; *Hochstaedter et al.*, 2001; Schmidt et al., manuscript in preparation, 2003]. Derivation of Nd in the Izu Volcanic Front rocks from the mantle wedge is consistent with Nd being relatively immobile in hydrous fluids [*Pearce et al.*, 1995], which are believed to be the primary

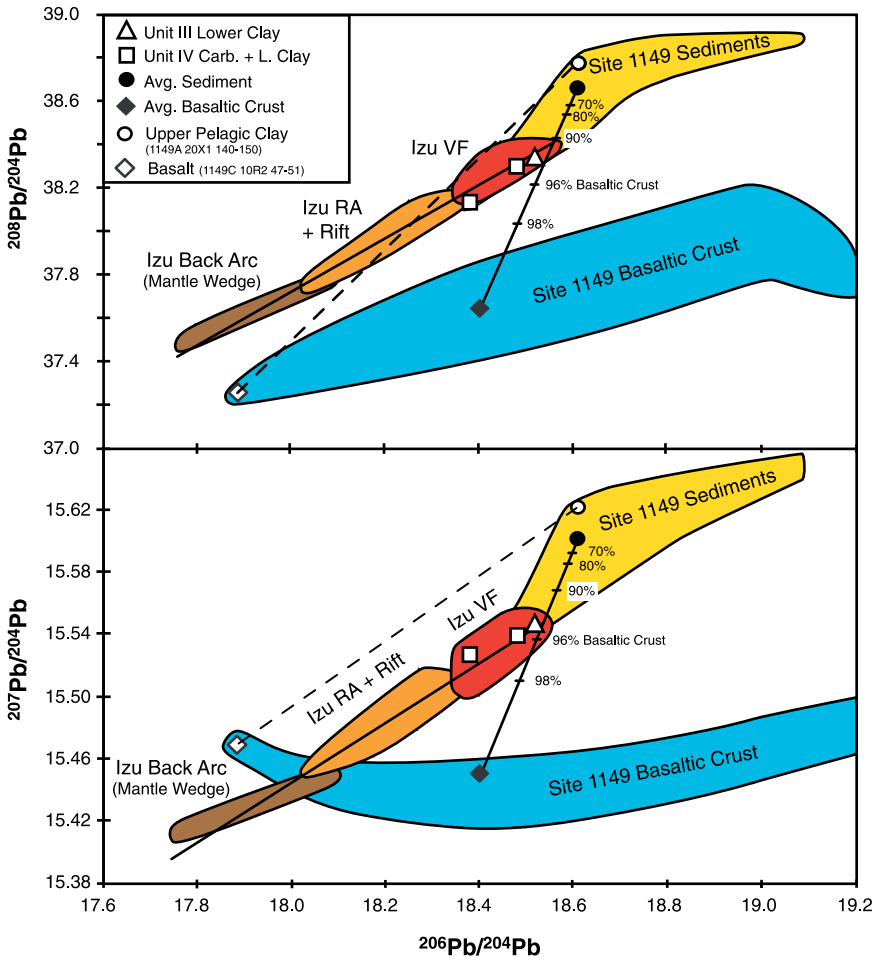

Figure 7. Pb isotope correlation diagrams showing input and output components of the Izu subduction system. The input components refer to average basaltic crust and sediments from ODP Site 1149 during this study. From the Site 1149 sediments, Unit III clay and Unit IV carbonates + clay are plotted separately as open symbols. The output components comprise Middle Miocene to Holocene Izu volcanic front (VF), rear arc + rift (RA) and back arc [*Hickey-Vargas*, 1991, 1998; Schmidt et al., manuscript in preparation, 2003]. The best fit line through the output data has excellent correlation coefficients of $r^2 = 0.90$ on the uranogenic diagram and $r^2 = 0.95$ on the thorogenic diagram consistent with two component mixing. While the unradiogenic end appears to represent the mantle wedge, the radiogenic end could either reflect lower sediments (Unit III clay and Unit IV carbonate with clay) or a mixture of average sediment and basaltic crust. A hypothetical mixing line (dashed) is shown for mixing of pelagic sediment and the most unradiogenic ocean crust sample. See text for details.

medium for transferring elements from the subducting slab to the source of the Izu Volcanic Front magmas [*Hochstaedter et al.*, 2001; *Taylor and Nesbitt*, 1998].

[40] The Pb isotopic composition of the Eocene through Holocene Izu Volcanic Front rocks, as well as the, rift, rear and back arc lavas, form remarkably linear trends with $r^2 = 0.90$ and 0.95 on the uranogenic and thorogenic diagrams respectively (Figure 7) implying that the Pb isotope systematics are controlled by the mixing of two components: (1) an unradiogenic end-member with $^{206}Pb/^{204}Pb \leq 17.75$, $^{207}Pb/^{204}Pb \leq 15.41$ and $^{208}Pb/^{204}Pb \leq 37.5$ and (2) a radiogenic end-member with $^{206}Pb/^{204}Pb \geq 18.56$, $^{207}Pb/^{204}Pb \geq 15.55$ and $^{208}Pb/^{204}Pb \geq 38.4$ (Schmidt et al., manuscript in preparation, 2003). Several mixing scenarios can explain the Pb-Pb isotope correlations of the Izu Arc volcanics. We consider the following possible end-members (1) mantle wedge, (2) average subducted sediment, (3) average subducted basaltic

ocean crust, (4) unaltered subducted ocean crust, and (5) lower clay from Unit III and IV. The following observations in Pb-Pb isotope space help to evaluate the role of these end-members in the Izu subduction factory (Figure 7). Although the Izu isotope array intersects the unradiogenic end of the field for igneous ocean crust at Site 1149 and Pacific MORB on the uranogenic Pb isotope diagram, it does not intersect either of these fields on the thorogenic Pb isotope diagram (Figure 7). All analyzed samples Site 1149 sediments have more radiogenic Pb than the unradiogenic end-member. Therefore the unradiogenic Pb component of the across arc Izu array is unlikely to have a subduction input origin. The less radiogenic end of the Izu Arc array (depleted Shikoku back arc basin samples) intersects the field for Indian MORB, indicating that the mantle wedge is the most likely source for the unradiogenic Pb component. The radiogenic end of the Izu Arc array intersects the field for sediments from Site 1149. Sediments can contain up to 20% water by volume [*Kastner et al.*, 1991] and therefore represent an important fluid source within subduction zones. Since Pb is highly fluid-mobile [*Pearce et al.*, 1995], Pb from the subducting slab is likely to be transported to the mantle wedge in a sediment-derived fluid. The extension of the Izu Arc Pb isotope array, however, does not intersect the average Site 1149 sediment composition, which is dominated by the upper clays due to their high Pb concentrations. As noted previously, clay-bearing carbonate samples from unit IV (samples 1149B 27R1 49–55 and 1149B 29R1 28–35) and clay from unit III (sample 1149B 12RCC 0–5) have Pb isotopic compositions that overlap with the Holocene Izu Volcanic Front rocks (Figure 7). Therefore the lower clay (since carbonate has very low concentrations of Pb) could be the primary (and possibly exclusive) source of the Pb in the Holocene Volcanic Front rocks, if a mechanism exists that only allows Pb from the lowermost portion of the sediment column (Unit IV and possibly the lower portions of Unit III) to reach the zone of melt generation. While removal (offscraping) of the uppermost sediment layers (clays and cherts of Units I through III) during subduction is possible, the Izu Arc shows no signs of accretion or underplating [*Taylor*, 1992] and thus subduction of the entire sediment package is assumed to be complete.

[41] ODP Leg 125 and 126 recovered serpentinite mounds that record the early dewatering of the subducting plate in the forearc [*Fryer et al.*, 1990; *Taylor et al.*, 1990]. Early dewatering was also observed in laboratory experiments that investigated the relative mobilities of trace elements in subduction zones [*You et al.*, 1996]. This study showed that Pb is readily mobilized as a result of the interaction of hydrothermal fluids with sediments at shallow (~10 km) depths. Since the Pb from the upper clays does not have the appropriate Pb isotopic composition to serve as the radiogenic end-member, the Pb from these clays may be released at shallow depths (e.g., in hydrothermal vents and serpentinite seamounts beneath the forearc), whereas the Pb from the lower clay within the carbonates (primarily Unit IV) may survive subduction to deeper depths, i.e., beneath the Izu Volcanic Front. Melting experiments and the occurrence of carbonate in high pressure metamorphic assemblages [*Canil and Scarfe*, 1990; *Becker and Altherr*, 1992; *Biellmann et al.*, 1993; *Yaxley and Green*, 1994] indicate that carbonates can survive subduction to pressures of 30–35 kb (depths of ~100 km) and to even higher pressures if they do not interact with hydrous fluids. Thermal models [*Rüpke et al.*, 2002] show that significant dehydration of the slab occurs beneath the volcanic front (30–35 kb), providing a source for the water. Therefore melting of the lower carbonate and liberation of the Pb within the clays is likely to primarily occur beneath the Volcanic Front. It is conceivable that the carbonates and possibly cherts prevent the release of at least some of the Pb from the lower clays until the subducting slab reaches ~100 km depths beneath the Izu Volcanic Front.

[42] Previous studies [e.g., *Hochstaedter et al.*, 2000, 1990] have proposed that replenishment within the Izu mantle wedge occurs through corner flow [*Spiegelman and McKenzie*, 1987], i.e., the asthenosphere flows along the base of the lithosphere into the subduction corner replacing asthenosphere and being dragged to depth by the subducting plate. If convection in the Izu Arc occurs through corner flow, the Pb in the mantle

wedge will be almost completely removed through melt generation in the back arc, rear arc and/or rift so that the asthenospheric mantle reaching the source of the Volcanic Front magmas will be highly depleted in Pb. Therefore Pb from the subducting slab (lower clays) could dominate the Pb budget of the Volcanic Front magmas, resulting in magmas with Pb isotopic compositions identical to the lower clays.

[43] Other investigators [e.g., *Ishikawa and Nakamura*, 1994; *Straub and Layne*, 2002], however, propose that fluids from the sediments and the altered oceanic crust mix to form a single homogeneous input component, which in turn mixes with the mantle wedge. An integrated slab component (or rather an additional input component) was necessary, because two component mixtures of sediments and the mantle wedge failed to intersect the arc volcanic rocks on Nd/Pb versus Pb isotope plots [*Miller et al.*, 1994]. We note, however, that the carbonates and lower clays have similar Nd/Pb [*Kelley et al.*, 2003], as well as Pb isotope ratios, to the Izu Volcanic Front rocks and therefore alleviate the necessity for an additional input component, but don't rule out a Pb contribution from the altered igneous crust. Indeed, modeling of the thermal regime in arcs shows that most of the water in the sediments will be released beneath the forearc but that most of the water in the altered igneous crust will be released beneath the Volcanic Front [*Rüpke et al.*, 2002]. Considering the high mobility of Pb in hot aqueous fluids, these fluids will undoubtedly transport a mixture of Pb from the subducting crust and sediments to the mantle wedge beneath the arc.

[44] Interestingly the mixing line between the average Site 1149 sediments and basaltic ocean crust intersect the radiogenic end of the Eocene through Holocene Izu Arc output array, which includes volcanic front, rift rear arc and back arc samples. The intersection of the average input mixing line with Izu volcanic Arc rocks yields an integrated slab component with with $^{206}Pb/^{204}Pb$ = 18.56, $^{207}Pb/^{204}Pb$ = 15.55 and $^{208}Pb/^{204}Pb$ = 38.40, representing a contribution of 90–95% Pb from the basaltic crust and 5–10% Pb from the sediments (Figure 7). Mixing of the integrated radiogenic slab component with the unradiogenic mantle wedge component can generate the Izu arc array. This mixing scenario is consistent with the linear array formed by the Izu arc volcanic rocks, even though three components (two slab and the mantle wedge) may contribute to the Izu output. We note that the Pb isotopic composition of many of the volcanic front samples (samples in the approximately lower right half of the volcanic front field) could be generated simply by mixing sediments (primarily upper pelagic clays) with basaltic crust of variable composition with $^{206}Pb/^{204}Pb \leq 18.4$ (value of average basaltic crust) and thus don't require Pb from the mantle wedge. It is however not possible to generate the complete Pb isotopic compositions of some volcanic front samples (samples in the upper left hand half of the volcanic front field), rift, rear arc and back arc solely by mixing one of the analyzed sediments with one of the ocean crust samples. This is illustrated in Figure 7 by a mixing line joining an upper pelagic sediment with the ocean crust sample with the least radiogenic Pb. Although the mixing line intersects the least radiogenic end of the Volcanic Front field on the thorogenic Pb diagram, it plots well above all Izu arc samples on the uranogenic diagram. In conclusion, both types of models discussed above (1) delayed dewatering of lower sediment column and (2) mixing of integrated slab fluid with mantle wedge - can successfully generate the Pb isotopic composition of the Volcanic Front lavas but require the Pb in the Izu Volcanic Front lavas to be dominated (if not exclusively controlled) by the input into the subduction zone. Interestingly in accordance with the first model, the Pb in the arc rocks comes almost exclusively from the lower sediment column; whereas in accordance with the second model, the Pb in the integrated slab fluid primarily comes from the altered basaltic crust. In order to derive the Pb concentrations in the Izu Volcanic Front rocks in the second model, the extremely high Pb concentration in the slab fluid must be mixed with $\geq$98% melt from the mantle wedge (Schmidt et al., manuscript in preparation, 2003).

[45] One of the surprising aspects of the Izu Eocene through Holocene Arc rocks is that their

Pb isotopic compositions fall on binary mixing lines on both Pb isotope correlation diagrams indicating that the composition of the end-members has remained relatively constant throughout the lifespan of the arc and across the entire arc, although there have been temporal and spatial variations in the mixing proportions. If the Pb from the input beneath the entire arc and throughout the history of the arc is almost exclusively derived from a single component (the lower clays), then it is easy to fix the input composition through time. Nevertheless, it is difficult to explain why Pb from the subducting igneous crust does not contribute to the fluids from the subducting slab. Considering the large range in Pb isotopic composition of the input (both sediments and igneous crust), the integrated slab component model requires that the slab fluid samples and mixes the diverse components within the subducting slab in such a way that an almost identical composition is produced through time. This criteria could be fulfilled in a steady state system in which tectonic parameters, such as slab dip and subduction rate, and the composition of the input remain relatively constant through time. Since the magnetic lineations on the subducting seafloor are roughly perpendicular to the trench, crust of similar age could have subducted beneath the Izu Arc through time and therefore the composition of the input may also have remained relatively constant through time. More detailed work and evaluation of the Izu arc output is necessary to distinguish between these end-member scenarios. In conclusion this study shows a clear link between Pb isotopic composition of the input and the Izu Arc output.

3.2.2. Mariana Arc

[46] The geochemistry of the Mariana Volcanic Front was studied in detail by *Elliott et al.* [1997], who identified two discrete slab components in the Mariana Arc volcanic rocks: (1) melt from subducted sediments, and (2) aqueous fluids derived from the subducted altered igneous crust. On the Pb isotope correlation diagrams (Figure 8), the Mariana's Volcanic Front data form a steep array with a positive slope. The most significant differences in the sediment input at the Mariana as compared to the Izu subduction system are (1) the presence of volcaniclastic turbidites, associated with intraplate volcanism, outboard the Mariana Arc, and (2) the absence of carbonates at the base of the sediment sequence. Both of these factors contribute to the more radiogenic Pb isotopic composition of the average sediment column drilled during ODP Leg 129 [*Plank and Langmuir*, 1998] compared to our average for Site 1149 (Table 3). The average sediment content estimated from ODP Leg 129 plots at the radiogenic end of the Pb isotope array for the Mariana Arc volcanic rocks. The $^{206}Pb/^{204}Pb$ isotopic composition of the ~440 m altered igneous basement at Site 801, however, is too high to serve as the unradiogenic component (Figure 8 and Table 5). One possibility to generate the unradiogenic end of the Mariana Pb isotope array is to mix 801C average altered igneous crust with depleted Indian-type mantle wedge. As shown in Figure 8 this translates to ~88% of the unradiogenic Pb to originate from the mantle wedge and ~12% from the altered upper ocean crust. An important prerequisite for this mixing sequence is that Pb from the upper ocean crust first mixes with the mantle wedge and then with sediment melts. Because fluids from the upper igneous ocean crust will pass through the overlying sediments before they reach the mantle wedge, it is difficult to visualize a scenario in which ocean crust fluids mix with the mantle wedge first. Therefore it is unlikely that that the mantle wedge beneath the Marianas contributes significantly to the Pb isotope budget of the Mariana volcanic output. The oceanic crust, nonetheless, also consists of unaltered portions that should have a similar composition to Pacific MORB at 167 Ma. As is illustrated in Figure 8, a mixture of ~80–84% unaltered ocean crust and ~20–16% average basaltic crust (similar in composition to the average Site 801 crust) has a composition that could serve as the unradiogenic end-member for the Mariana Arc volcanic rocks.

[47] Several problems still need to be considered in light of these mixing proportions. Assuming an average thickness of 7 km for the subducting crust, then ~1.4 km of altered basement with a composition similar to the average for Site 801 and ~5.6 km of unaltered crust would contribute Pb to the fluids generated from the igneous crust.

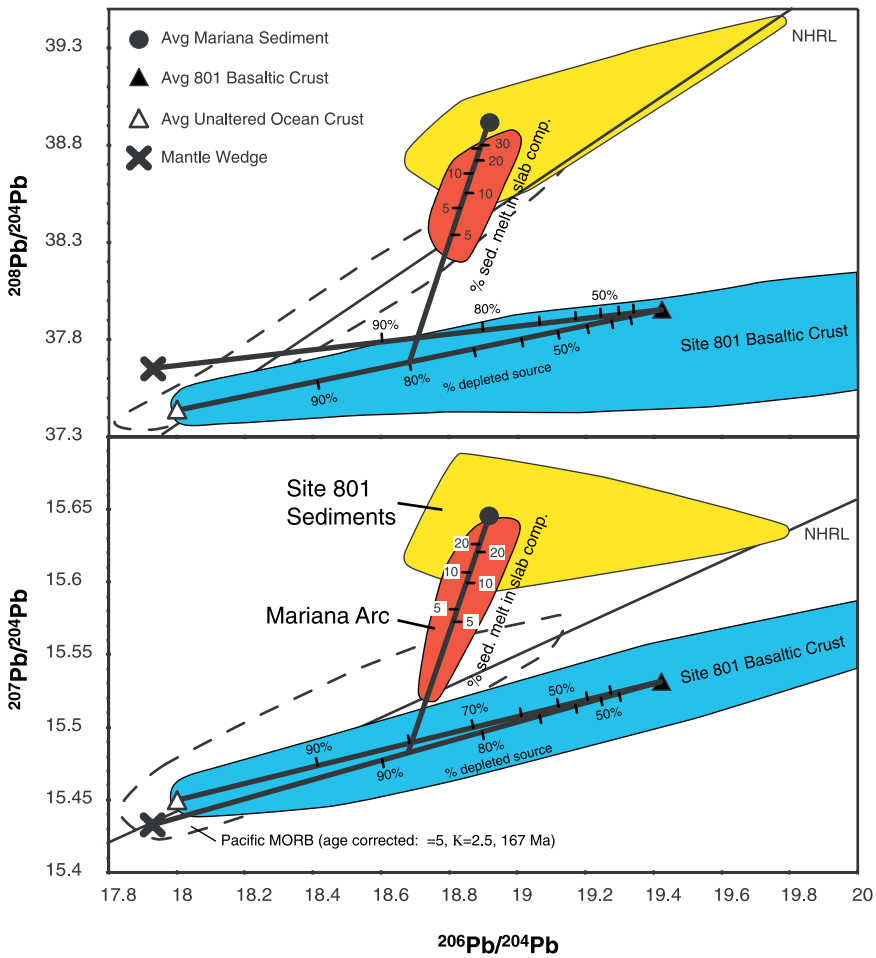

Figure 8. Pb isotope mixing relations of input and output components for the Mariana arc. Average sediment and sediment field after *Plank and Langmuir* [1998]. Field for basaltic crust and average of the basaltic crust refer to ODP Site 801 from this study. The Pb isotope data of the Mariana arc [*Elliott et al.*, 1997] lies on a mixing line between average sediment and mixture of ~80–86% unaltered ocean crust and ~20–16% highly altered crust. A possible mixing line is shown for mixing of mantle wedge with average basaltic crust. See text for discussion.

Generally the zone of alteration extends to deeper depths than 1.4 km within the ocean crust. Nevertheless it is to be expected that the effects of alteration will decrease with depth in the crust and therefore the crust beneath the ~500 m drilled at Site 801 will have intermediate isotopic composition between the two end-members considered in our calculations, assuming that our Site 801 average for the basaltic crust is not biased by alteration products. Alternatively some of the Pb from the uppermost crust may have been lost beneath the forearc and therefore no longer be available beneath the Volcanic Front. In either case, it is necessary to extract Pb from unaltered (lower) portions of the crust. This is only possible if there is a source of hydrous fluids within the lower oceanic crust or within the uppermost subducting lithospheric mantle. As a result of the steep (nearly vertical) subduction of the Pacific Plate beneath the Mariana Arc, the subducting plate is strongly flexed outboard of the trench. In response to such flexure, deep normal faults are likely to form, which could allow seawater to reach and serpentinize the uppermost mantle beneath the subducting crust [*Ranero et al.*, 2001; *Rüpke et al.*, 2002; *Stern and Klemperer*, 2003]. Fluids from serpentinite in the subducting slab will not be released until higher P-T conditions than the fluids from the altered oceanic crust. Considering the steep subduction angle of the Pacific Plate beneath the Mariana

Arc, fluids from the serpentinite at the base of the crust are likely to rise beneath the Volcanic Front and mix with fluids from the upper altered oceanic crust, efficiently homogenizing the Pb from the entire subducting oceanic crust (upper and lower portions) and also from the uppermost serpentinized lithospheric mantle. The steep subduction angle beneath the Mariana Arc will also allow sediment melts to ascend beneath the volcanic front mixing with fluids from the crust, which does not appear to be the case at the Izu arc [*Taylor and Nesbitt*, 1998; *Hochstaedter et al.*, 2001; Schmidt et al., manuscript in preparation, 2003] The mixing calculations show that the Pb in the Mariana Arc rocks can be derived from 3 to nearly 100% melts from subducted sediment with the remainder coming from an integrated fluid from the subducting igneous crust (Figure 8).

[48] In contrast to the Mariana Arc, the shallower subduction angle of 60–70° beneath the Izu Arc does not cause the plate to bend as extensively and therefore "bend faults" are less likely, which allow water to serpentinize the uppermost mantle of the subducting slab. Therefore the main sources of fluids beneath the Izu Volcanic Front are likely to be the lower carbonate sediments and the uppermost igneous crust. The flatter subduction angle does not generate a P-T regime in which sediments melt or serpentinite in the subducting lithospheric mantle is dehydrated until the subducting plate reaches depths beneath the rear and/or back arc. In conclusion, we propose that the input and structure (i.e., slab dip) control the composition of the output of the Izu and Mariana Arcs.

3.3. Implications for the Deep Recycling of Oceanic Crust

[49] Three samples from Site 801C igneous crust, each of which contained carbonate, yielded extremely radiogenic $^{206}Pb/^{204}Pb$ (23.7–26.9) and $^{207}Pb/^{204}Pb$ (15.73–15.83) but relatively unradiogenic $^{208}Pb/^{204}Pb$ (37.5–38.7). The $^{206}Pb/^{204}Pb$ isotope ratios are more radiogenic, the $^{207}Pb/^{204}Pb$ are similar and the $^{208}Pb/^{204}Pb$ is lower than found in end-member HIMU ocean island basalts from Mangaia, Tubaii and St. Helena (20.5–21.7; 15.71–15.83; 39.7–40.6, respectively). The average Pb isotopic composition of the Site 801C basement has similar $^{206}Pb/^{204}Pb$ (21.0) but significantly lower $^{207}Pb/^{204}Pb$ (15.59) and $^{208}Pb/^{204}Pb$ (38.1). Below we explore the Pb isotopic evolution of Site 801C ocean crust after subduction and its relation to HIMU, commonly thought to represent 1.8 Ga old recycled ocean crust.

[50] Upon subduction, the Th/U ratio in the residual crust is likely to be raised considerably. This is evident from the higher fluid mobility of U compared to Th and is observed in ^{238}U enrichment relative to ^{230}Th in Mariana lavas [*Elliott et al.*, 1997]. Pb is generally considered to be more mobile in subduction zone fluids than U and therefore U/Pb is likely to increase in the residual subducted slab. Given sufficient time, the residual slab will also evolve high $^{208}Pb/^{204}Pb$ isotope ratios and still higher $^{206}Pb/^{204}Pb$ and $^{207}Pb/^{204}Pb$. If this scenario is applied to ODP Site 801 ocean crust, we observe that at recycling times of several billion years, the recycled ocean crust component will develop Pb isotope ratios, that are distinct from the HIMU end-member presently observed in ocean island volcanic rocks. Namely it will have extremely high $^{206}Pb/^{204}Pb$ relative to $^{207}Pb/^{204}Pb$ due to today's high $^{238}U/^{235}U$ of 137.66 reflecting the ~6.5 times shorter half live of ^{235}U than ^{238}U.

[51] The results from this study contrast with those from Jurassic (~170 Ma) Atlantic Ocean crust near the NW African continental margin at the Canary Islands [*Hoernle*, 1998]. Here one sample from the ocean crust on which the Canary Islands are located had identical $^{206}Pb/^{204}Pb$ (20.73) and $^{207}Pb/^{204}Pb$ (15.73) to lavas from St. Helena, the Atlantic HIMU end-member. The $^{208}Pb/^{204}Pb$ ratio (41.3) was considerably higher than at St. Helena, but similar to Cameroon Line HIMU. In order to explain the high $^{207}Pb/^{204}Pb$ in all Jurassic Atlantic samples, hydrothermal exchange of Pb in the basaltic crust with Pb from sediments during formation of the crust was invoked that will raise $^{207}Pb/^{204}Pb$ and $^{208}Pb/^{204}Pb$ and leave $^{206}Pb/^{204}Pb$ relatively unchanged. Hydrothermal alteration can also increase the U/Pb ratio by leaching of Pb as evident by high Ce/Pb and Nd/Pb in HIMU basalts. Low temperature alteration increases U/Pb by addition of U which also causes HIMU like

$^{206}Pb/^{204}Pb$ ratios even after 170 Ma if μ is high enough (e.g., >100). If this HIMU like Pb is reintroduced into the mantle it is one possibility to replenish the HIMU reservoir without the necessity for several billion years of recycling time. The complex Pb evolution observed in Jurassic Atlantic MORB no doubt reflects the proximity of the ocean crust beneath Gran Canaria to a continental margin and a thick continental rise sedimentary sequence above this crust even during the initial opening of the Atlantic, in contrast to the more oceanic settings for Site 1149 and 801 at their formation. Considering the extreme heterogeneity in Pb isotopic composition found in both Mesozoic Pacific and Atlantic crust, it is surprising that the HIMU components in ocean islands are so uniform in their uranogenic and thorogenic Pb isotopic compositions. Of course Early Cretaceous to Jurassic (~130–170 Ma) oceanic crust clearly serves as an end-member for oceanic crust. On average subducted crust will be far younger and thus less heterogeneous in Pb isotopic composition.

4. Conclusions

[52] The Sr-Nd-Pb isotopic composition of 10 sediment samples and 18 igneous basement samples from ODP Site 1149 and 801 located in front of the Izu and Mariana arcs were investigated in order to characterize the composition and evolution of Mesozoic oceanic crust and to constrain the unmodified input into these subduction zones. Our results show that:

[53] 1. On the basis of mineralogy and Sr-Nd-Pb isotopic composition, five different sediment end-members are identified in the sediment column of Site 1149: (1) upper clay from Units I and II, (2) volcanic ash from Unit I, (3) chert from Unit III, (4) lower clay from lower Unit III and Unit IV, (5) carbonate from Unit IV.

[54] 2. The increase of $^{87}Sr/^{86}Sr$ in the clays and cherts from Unit 1 to Unit II to Unit III could either reflect a change toward more continental sources or the increasing $^{87}Rb/^{86}Sr$ ratios downsection.

[55] 3. The variation in Pb isotopic composition of the sediments is greater than previously reported from this area.

[56] 4. Owing to high Pb contents, the upper pelagic clays dominate the average Pb isotopic composition of the sediments which does not lie on the radiogenic end of the mixing array of the Izu arc.

[57] 5. The Pb isotopes of the lower clays (Unit III) and carbonates with clay (Unit IV) are distinct from the upper clays and overlap with those from the Izu Volcanic Front.

[58] 6. $^{143}Nd/^{144}Nd$ ratios of the igneous basement at both Sites are consistent with derivation from a depleted upper mantle source except for an alkali basalt at Site 801 that formed from a plume-type mantle source 10 Ma after ocean crust formation. Highly variable $^{87}Sr/^{86}Sr$ ratios at near constant $^{143}Nd/^{144}Nd$ requires addition of Sr derived seawater to the igneous crust.

[59] 7. Within the U-Th-Pb isotope system $^{206}Pb/^{204}Pb$ ratios show the strongest effect of seawater interaction that increases $^{238}U/^{204}Pb$ and leads to highly variable $^{206}Pb/^{204}Pb$ ratios (17.88–26.86) with time. $^{207}Pb/^{204}Pb$ and $^{208}Pb/^{204}Pb$ ratios are less variable reflecting the low abundance of ^{235}U in natural samples and the immobility of Th and Pb during low temperature seawater alteration respectively.

[60] 8. Initial Pb isotopes of most samples broadly overlap with the age-corrected field of the Pacific MORB source indicating that in most cases the increase of $^{238}U/^{204}Pb$ occurred within a few Ma after formation of the crust and that the Pacific MORB source evolved primarily through in situ radioactive decay over the last ~170 Ma.

[61] 9. The Pb isotopic composition of the Izu and Mariana subduction zone output implies a two component mixing scenario. While the Pb isotope array of the Izu arc involves an Indian-MORB-type mantle wedge component on the unradiogenic side and an input derived component on the radiogenic side, both mixing end-members appear to be input derived at the Marianas. The mixing proportions of an integrated slab component responsible for the radiogenic end-member of the Izu arc requires 90–94% of the Pb to be derived from the basaltic crust and 4–10% of the Pb to come from the sediments.

Mixing of ≥98% mantle wedge melts with this slab fluid is necessary to obtain the Pb concentrations observed in the lavas of the Izu Arc. Alternatively, only a single lower sediment component is required. Delayed dewatering of the lower sediment column could transfer the Pb isotope signal of the lower carbonate + clay directly into the melt zone of the Izu Volcanic Front. Mixing calculations for the Marianas indicate that ~80–86% of the unradiogenic Pb component comes from unaltered crust and ~20–16% of the Pb from highly altered. Extraction of unaltered Pb from the deep crust is believed to reflect dewatering of serpentinized upper mantle. Mantle serpentinization could be a consequence of vertical bending of the subducting slab beneath the Mariana arc that causes deep faulting followed by deep fluid migration. The unradiogenic component mixes with ~3 to nearly 100% sediment component to form the Mariana Pb isotope mixing array.

[62] 10. Despite the extremely radiogenic Pb isotopic compositions some Site 801 ocean crust samples, this crust does not have combined $^{206}Pb/^{204}Pb$, $^{207}Pb/^{204}Pb$ and $^{208}Pb/^{204}Pb$ HIMU-type isotopic compositions and will not in the future either.

Acknowledgments

[63] Samples were provided by the Ocean Drilling Program (ODP), sponsored by the U.S. National Science Foundation (NSF) and participating countries under management of Joint Oceanographic Institutions (JOI), Inc. We thank Silke Vetter for carrying out some of the isotope analyses and Susanne Straub for help in acquiring funding. Especial thanks go to Katherine Kelley and Terry Plank for allowing us to use their unpublished trace element data upon which many of the major conclusions of this paper are critically dependent. We want to thank Jim Gill, Terry Plank, Bill White (editor), John Ludden (associate editor), Pat Castillo (reviewer) and an anonymous reviewer for their constructive and stimulating comments that improved the initial version of this paper. The German Science Foundation (DFG) funded this research through grant Ho 1833/7-1. This publication is contribution no. 19 of the Sonderforschungsbereich 574 "Volatiles and Fluids in Subduction Zones" at Kiel University.

References

Abrams, L., Correlation among core, logging, and seismic data at Site 1149 in the Nadezha Basin, *Proc. Ocean Drill. Program Sci. Res.*, *185*, 2002. (Available at http://www-odp.tamu.edu/publications/185_SR/001/001.htm)

Abrams, L. J., R. L. Larson, T. H. Shipley, and Y. Lancelot, Cretaceous volcanic sequences and Jurassic oceanic crust In the East Mariana and Pigafetta basins of the Western Pacific, in *The Mesozoic Pacific: Geology, Tectonics, and Volcanism*, *Geophys. Monogr. Ser.*, vol. 77, edited by M. S. Pringle et al., pp. 77–101, AGU, Washington, D. C., 1993.

Bartolini, A., and R. Larson, Pacific microplate and the Pangea supercontinent in the Early to Middle Jurassic, *Geology*, *29*, 735–738, 2001.

Becker, H., and R. Altherr, Evidence from ultra-high-pressure marbles for recycling of sediments into the mantle, *Nature*, *358*, 745–748, 1992.

Biellmann, C., P. Gillet, F. Guyot, J. Peyronneau, and B. Reynard, Experimental evidence for carbonate stability in the Earth's lower mantle, *Earth Planet. Sci. Lett.*, *118*, 31–41, 1993.

Brenan, J. M., H. F. Shaw, and F. J. Ryerson, Experimental evidence for the origin of lead enrichment in convergent-margin magmas, *Nature*, *378*, 54–56, 1995a.

Brenan, J. M., H. F. Shaw, F. J. Ryerson, and D. L. Phinney, Mineral-aqueous fluid partitioning of trace elements at 900°C and 2.0 GPa: Constraints on the trace element chemistry of mantle and deep crustal fluids, *Geochim. Cosmochim. Acta*, *59*, 3331–3350, 1995b.

Canil, D., and C. M. Scarfe, Phase relations in peridotite + CO2 systems to 12 GPa: Implications for the origin of kimberlite and carbonate stability in the earth's upper mantle, *J. Geophys. Res.*, *95*, 15,805–15,816, 1990.

Carlson, R. L., and M. Mortera-Gutierrez, Subduction hinge migration along the Izu-Bonin-Mariana Arc, *Tectonophysics*, *181*, 331–344, 1990.

Castillo, P. R., P. A. Floyd, and C. France-Lanord, Isotopic geochemistry of Leg 129 basalts: Implications for the origin of the widespread cretaceous volcanic event in the Pacific, *Proc. Ocean Drill. Program Sci. Res.*, *129*, 405–413, 1992a.

Castillo, P. R., P. A. Floyd, C. France-Lanord, and J. C. Alt, Data Report: Summary of geochemical data for Leg 129 Igneous rocks, *Proc. Ocean Drill. Program Sci. Res.*, vol. 129, 653–670, 1992b.

Chan, L. H., W. P. Leeman, and C.-F. You, Lithium isotopic composition of Central American Volcanic Arc lavas: Implications for modification of subarc mantle by slab-derived fluids, *Chem. Geol.*, *160*, 255–280, 1999.

Channell, J. E. T., E. Erba, M. Nakanishi, and K. Tamaki, Late Jurassic-Early Cretaceous time scales and oceanic magnetic anomaly block models, in *Geochronology, Time Scales and Global Stratigraphic Correlations*, edited by W. A. Berggren et al., *Spec. Publ. Soc. Econ. Paleontol. Mineral.*, *54*, 51–63, 1995.

Chiu, J. M., B. L. Isacks, and R. K. Cardwell, 3-D configuration of subducted lithosphere in the western Pacific, *Geophys. J. Int.*, *106*, 99–111, 1991.

Class, C., D. M. Miller, S. L. Goldstein, and C. H. Langmuir, Distinguishing melt and fluid subduction components in Umnak volcanics, Aleutian arc, *Geochem. Geophys. Geosyst.*, *1*, Paper number 1999GC000010, 2000.

Crawford, A. J., L. Beccaluva, and G. Serri, Tectono-magmatic evolution of the West Philippine-Mariana region and the origin of boninites, *Earth Planet. Sci. Lett.*, *54*, 346–356, 1981.

DeMets, C., R. G. Gordon, D. F. Argus, and S. Stein, Current plate motions, *Geophys. J. Int.*, *101*, 425–478, 1990.

Elderfield, H., Strontium Isotope Stratigraphy, *Paleogeogr. Palaeoclimatol. Palaeoecol.*, *57*, 71–90, 1986.

Elliott, T., T. Plank, A. Zindler, W. White, and B. Bourdon, Element transport from slab to volcanic front at the Mariana arc, *J. Geophys. Res.*, *102*, 14,991–15,019, 1997.

Faure, G., *Principles of Isotope Geology*, 589 pp., John Wiley, Hoboken, N. J., 1986.

Fryer, P., et al., *Proceedings of the Ocean Drilling Program, Inital Reports*, *125*, 1092 pp., Ocean Drill. Program, College Station, Tex., 1990.

Gill, J. B., C. Seales, P. Thompson, A. G. Hochstaedter, and C. Dunlap, Petrology and geochemistry of pliocene-pleistocene volcanic rocks from the Izu arc, Leg 126, *Proc. Ocean Drill. Program Sci. Res.*, *126*, 383–404, 1992.

Hauff, F., K. Hoernle, G. Tilton, D. Graham, and A. C. Kerr, Large volume recycling of oceanic lithosphere: Geochemical evidence from the Caribbean large igneous province, *Earth Planet. Sci. Lett.*, *174*, 247–263, 2000a.

Hauff, F., K. Hoernle, and P. van den Bogaard, Age and geochemistry of basaltic complexes to the geotectonic evolution of Central America, *Geochem. Geophys. Geosyst.*, *1*, Paper number 1999GC000020, 2000b.

Hawkesworth, C., and R. Ellam, Chemcial fluxes and wedge replenishment rates along recent destructive plate margins, *Geology*, *17*, 46–49, 1989.

Hawkesworth, C. J., J. M. Hergt, R. M. Ellam, and F. McDermott, Element fluxes associated with subduction related magmatism, *Philos. Trans. R. Soc. London*, *335*, 393–405, 1991.

Hickey-Vargas, R., Isotope characteristics of submarine lavas from the Philippine Sea: Implications for the origin of arc and basin magmas of the Philippine tectonic plate, *Earth Planet. Sci. Lett.*, *107*, 290–304, 1991.

Hickey-Vargas, R., Origin of the Indian Ocean-type isotopic signature in basalts from the Phillipine Sea plate spreading centers: An assasment of local versus large-scale processes, *J. Geophys. Res.*, *103*, 20,963–20,979, 1998.

Hochstaedter, A. G., J. B. Gill, and J. D. Morris, Volcanism in the Sumisu Rift: II. Subduction and non-subduction related components, *Earth Planet. Sci. Lett.*, *100*, 195–209, 1990.

Hochstaedter, A. G., J. B. Gill, O. Ishizuka, M. Yuasa, and M. Sumito, Across-arc geochemical trends in the Izu-Bonin arc: Constraints on source composition and mantle melting, *J. Geophys. Res.*, *105*, 495–512, 2000.

Hochstaedter, A., J. Gill, R. Peters, P. Broughton, P. Holden, and B. Taylor, Across-arc geochemical trends in the Izu-Bonin arc: Contributions from the subducting slab, *Geochem. Geophys. Geosyst.*, *2*, Paper number 2000GC000105, 2001.

Hoernle, K., Geochemistry of Jurassic oceanic crust beneath Gran Canaria (Canary Islands): Implications for crustal recycling and assimilation, *J. Petrol.*, *39*, 859–880, 1998.

Hoernle, K. A., and G. R. Tilton, Sr-Nd-Pb isotope data for Fuerteventura (Canary Islands) basal complex and subaerial volcanics: Application to magma genesis and evolution, *Schweiz. Mineral. Petrogr. Mitt.*, *71*, 3–18, 1991.

Hole, M. J., A. D. Saunders, G. F. Marriner, and J. Tarney, Subduction of pelagic sediments: Implications for the origin of Ce-anomalous basalts from the Mariana Islands, *J. Geol. Soc. London*, *141*, 453–472, 1984.

Ingram, B. L., Ichthyolith Strontium isotopic stratigraphy of deep-sea clays: Sites 885 and 886 (North Pacific Transect), *Proc. Ocean Drill. Program Sci. Res.*, *145*, 399–406, 1995.

Ishikawa, T., and E. Nakamura, Origin of the slab component in arc lavas from across-arc variation of B and Pb isotopes, *Nature*, *370*, 205–208, 1994.

Ishikawa, T., and F. Tera, Two isotopically distinct fluid components involved in the Mariana arc: Evidence from Nb/B ratios and B, Sr, Nd and Pb isotope systematics, *Geology*, *27*, 83–86, 1999.

Ito, E., W. M. White, and C. Göpel, The O, Sr, Nd and Pb isotope geochemistry of MORB, *Chem. Geol.*, *62*, 157–176, 1987.

Janney, P. E., and P. R. Castillo, Basalts from the Central Pacific Basin: Evidence for the origin of Cretaceous igneous complexes in the Jurassic western Pacific, *J. Geophys. Res.*, *101*, 2875–2893, 1996.

Janney, P. E., and P. R. Castillo, Geochemistry of Mesozoic Pacific mid-ocean ridge basalt: Constraints on melt generation and the evolution of the Pacific upper mantle, *J. Geophys. Res.*, *102*, 5207–5229, 1997.

Kastner, M., H. Elderfield, and J. M. Martin, Fluids in convergent margins: What do we know about their composition, origin, role in diagenesis and importance for oceanic chemical fluxes?, *Philos. Trans. R. Soc. London*, *335*, 243–259, 1991.

Kelley, K. A., T. Plank, J. Ludden, and H. Staudigel, The composition of altered oceanic crust at ODP Sites 801 and 1149, *Geochem. Geophys. Geosyst.*, *4*(6), 8910, doi:10.1029/2002GC000435, 2003.

Kosigo, T., Y. Tatsumi, and S. Nakano, Trace element transport during dehydration processes in the subducted oceanic crust: 1. Experiments and implications for the origin of ocean basalts, *Earth Planet. Sci. Lett.*, *148*, 193–205, 1997.

Lancelot, Y., et al., *Proceedings Ocean Drilling Program Inital Reports*, vol. 129, 488 pp., Ocean Drilling Program, College Station, Tex., 1990.

Lee, J. M., R. J. Stern, and S. H. Bloomer, Forty million years of magmatic evolution in the Mariana arc: The tephra record, *J. Geophys. Res.*, *100*, 17,671–17,687, 1995.

Lin, P.-N., Trace element and isotopic characteristics of western Pacific pelagic sediments: Implications for the petrogenesis of Mariana Arc magmas, *Geochim. Cosmochim. Acta*, *56*, 1641–1654, 1992.

Matsuoka, A., Jurassic and early cretaceous radiolarians from Leg 129, Sites 800 and 801, Western Pacific, *Proc. Ocean Drill. Program Sci. Res.*, *126*, 203–220, 1992.

Miller, D. M., S. L. Goldstein, and C. H. Langmuir, Cerium/lead and lead isotope ratios in arc magmas and the enrichment of lead in the continents, *Nature*, *368*, 514–520, 1994.

Morris, J. D., W. P. Leeman, and F. Tera, The subducted component in island arc lavas: Constraints from Be isotopes and B-Be systematics, *Nature*, *344*, 31–36, 1990.

Nakanishi, M., K. Tamaki, and K. Kobayashi, Mesozoic Magnetic Anomaly Lineations and Seafloor Spreading History of the Northwestern Pacific, *J. Geophys. Res.*, *94*, 15,437–15,462, 1989.

Nakanishi, M., K. Tamaki, and K. Kobayashi, A new mesozoic isochron chart of the northwestern Pacific Ocean: Paleomagnetic and tectonic implications, *Geophys. Res. Lett.*, *19*, 693–696, 1992.

Ogg, J. G., S. M. Karl, and R. J. Behl, Jurassic through Early Cretaceous sedimentation history of the Central Equatorial Pacific and Sites 800 and 801, *Proc. Ocean Drill. Program Sci. Res.*, *126*, 571–613, 1992.

Pearce, J. A., P. E. Baker, P. K. Harvey, and I. W. Luff, Geochemical evidence for subduction fluxes, mantle melting and fractional crystallization beneath the South Sandwich Island Arc, *J. Petrol.*, *36*, 1073–1109, 1995.

Pearce, J. A., P. D. Kempton, G. M. Nowell, and S. R. Noble, Hf-Nd element and isotope perspective on the nature and provenance of mantle and subduction components in Western Pacific arc-basin systems, *J. Petrol.*, *40*, 1579–1611, 1999.

Plank, T., and C. H. Langmuir, Tracing trace elements from sediment input to volcanic output at subduction zones, *Nature*, *362*, 739–743, 1993.

Plank, T., and C. H. Langmuir, The geochemical compostion of subducting sediment and its consequences for the crust and the mantle, *Chem. Geol.*, *145*, 325–394, 1998.

Plank, T., et al., *Proceedings Ocean Drilling Program*, *Inital Reports* [CD-ROM], vol. 185, Ocean Drill. Program, College Station, Tex., 2000.

PLATES Project, Atlas of paleogeographic reconstructions (PLATES Progress Report No. 215), *Tech. Rep. 181*, Univ. Tex., Inst. Geophys., Austin, 1998.

Pringle, M. S., Radiometric ages of basaltic basement recovered at Sites 800, 801, and 802, Leg 129, western Pacific Ocean, *Proc. Ocean Drill. Program Sci. Res.*, *129*, 389–404, 1992.

Ranero, C. R., J. P. Morgan, K. D. McIntosh, and C. Reichert, Flexural faulting and mantle serpentinization at the Middle American trench, *Eos Trans. AGU*, *82*(47), Fall Meet. Suppl., Abstract T22D-04, 2001.

Rüpke, L., J. P. Morgan, M. Hort, and J. A. D. Connolly, Are the regional variations in Central American arc lavas due to differing basaltic versus peridotitic slab sources of fluids?, *Geology*, *30*, 1035–1038, 2002.

Seno, T., S. Stein, and A. E. Gripp, A model for the motion of the Philippine sea plate consistent with Nuvel-1 and geological data, *J. Geophys. Res.*, *98*, 17,941–17,948, 1993.

Spiegelman, M., and D. McKenzie, Simple 2–D models for melt extraction at mid-ocean ridges and island arcs, *Earth. Planet. Sci. Lett.*, *83*, 137–152, 1987.

Stern, R. J., and F. M. J. Klemperer, An overview of the Izu-Bonin-Mariana Subduction Factory, in *The Subduction Factory*, *Geophys. Monogr. Ser.*, AGU, Washington, D. C., in press, 2003.

Stern, R. J., S. H. Bloomer, P.-N. Lin, E. Ito, and J. Morris, Shoshonitic magmas in nascent arcs: New evidence from submarine volcanoes in the northern Marianas, *Geology*, *16*, 426–430, 1988.

Straub, S. M., and G. D. Layne, The systematics of boron isotopes in Izu arc front volcanic rocks, *Earth Planet. Sci. Lett.*, *198*, 25–39, 2002.

Taylor, B., Rifting and the volcanic-tectonic evolution of the Izu-Bonin-Mariana Arc, *Proc. Ocean Drill. Program Sci. Res.*, *126*, 627–651, 1992.

Taylor, B., et al., *Proceedings Ocean Drilling Program Inital Reports*, vol. 126, 1002 pp., Ocean Drill. Program, College Station, Tex., 1990.

Taylor, R. N., and R. W. Nesbitt, Isotopic characteristics of subduction fluids in an intra-oceanic setting, Izu-Bonin Arc, Japan, *Earth Planet. Sci. Lett.*, *164*, 79–98, 1998.

Taylor, R. N., H. Lapierre, P. Vidal, R. W. Nesbitt, and I. W. Croudace, Igneous geochemistry and petrogenesis of the Izu-Bonin forearc basin, *Proc. Ocean Drill. Program Sci. Results*, *126*, 405–430, 1992.

Todt, W., R. A. Cliff, A. Hanser, and A. W. Hofmann, Evaluation of a ^{202}Pb-^{205}Pb Double Spike for High-Precision Lead Isotope Analysis, in *Earth Processes: Reading the Isotopic Code*, *Geophys. Monogr. Ser.*, vol. 95, edited by A. Basu and S. Hart, pp. 429–437, AGU, Washington, D. C., 1996.

Turner, S., C. Hawkesworth, N. Rogers, and P. King, U-Th isotope disequilibria and ocean island basalt generation in the Azores, *Chem. Geol.*, *139*, 145–164, 1997.

Van der Hilst, R., and T. Seno, Effects of relative plate motion on the deep structure and penetration depth of slabs below the Izu-Bonin and Mariana island arcs, *Earth Planet. Sci. Lett.*, *120*, 395–407, 1993.

Vroon, P. Z., M. J. van Bergen, G. J. Klaver, and W. M. White, Strontium, neodymium, and lead isotopic and trace-element signatures of the East Indonesian sediments: Provenance and implications for Banda Arc magma genesis, *Geochim. Cosmochim. Acta*, *59*, 2573–2598, 1995.

White, W. M., Isotopes and a smoking gun, *Nature*, *362*, 791–792, 1993.

White, W. M., A. W. Hofmann, and H. Puchelt, Isotope geochemistry of Pacific mid-ocean ridge basalts, *J. Geophys. Res.*, *92*, 4881–4893, 1987.

Woodhead, J. D., and D. G. Fraser, Pb, Sr and ^{10}Be isotopic studies of volcanic rocks from the Northern Mariana Islands. Implications for magma genesis and crustal recycling in the Western Pacific, *Geochim. Cosmochim. Acta*, *49*, 1925–1930, 1985.

Yaxley, G. M., and D. H. Green, Experimental demonstration of refractory carbonate-bearing eclogite and siliceous melt in the subduction regime, *Earth Planet. Sci. Lett.*, *128*, 313–325, 1994.

You, C.-F., P. R. Castillo, J. M. Gieskes, L. H. Chan, and A. J. Spivack, Trace element behaviour in hydrothermal experiments: Implications for fluid processes at shallow depths in subduction zones, *Earth Planet. Sci. Lett.*, *140*, 41–52, 1996.